Control Engineering Practice 21 (2013) 565–582

Contents lists available at SciVerse ScienceDirect

Control Engineering Practice

journal homepage: www.elsevier.com/locate/conengprac

Input observer convergence and robustness: Application to compression ratio estimation

Karla Stricker, Lyle Kocher, Dan Van Alstine, Gregory M. Shaver *

Purdue University, Department of Mechanical Engineering, Mechanical Engineering Building, Purdue University, West Lafayette, IN 47907, United States

ARTICLE INFO

Article history:
Received 5 March 2012
Accepted 26 November 2012
Available online 31 December 2012

Keywords:
Robust estimation
Estimators
Observers
Diesel engines
Variable valve timing

ABSTRACT

The focus of this paper is the analysis of a high-gain observer for estimating un-steady inputs, including guarantees for: (1) robustness to measurement uncertainty, and (2) transient upper bound on estimator error. A method for selecting the observer gain based on measurement uncertainty, acceptable steady-state errors, and desired estimation error convergence rates, is also described. This strategy is demonstrated in practice for internal combustion (IC) engine effective compression ratio (ECR) estimation. Experimental results are shown to be consistent with analytical guarantees—convergence within 4 engine cycles, and a steady-state error less than 0.5 ECR, in the presence of 10% measurement error.

© 2012 Elsevier Ltd. All rights reserved.

1. Introduction

High-gain observers have been used extensively in linear and non-linear estimation and control applications (Bullinger & Allgower, 1997; Chitour, 2002; Dabroom & Khalil, 1997; Gauthier & Kupka, 1994; Khalil, 1999, 2008; Mahmoud & Khalil, 2002; Poznyak, Martinez-Guerra, & Osorio-Cordero, 2000; Saberi & Sannuti, 1990; Veluvolu & Soh, 2009). In most cases, these are Luenberger-type estimators with a large gain, which are commonly used for estimation of slowly varying states or inputs. The effort by Stotsky and Kolmanovsky (Stotsky & Kolmanovsky, 2001, 2002; Stotsky, Kolmanovsky, & Eriksson, 2004) is one of the only strategies, to the authors' knowledge, that uses an auxiliary-variable high-gain observer approach to estimate unknown un-steady inputs. Several other efforts have also incorporated this approach (Ahn, Stefanopoulou, & Jankovic, 2009; Polushin, Liu, & Lung, 2008; Tona, Moulin, Venturi, Tilagone, & Gautier, 2007). This technique is desirable for dynamic, nonlinear systems in which the input to be estimated cannot be considered slowly varying. An effort detailed in Bartolini, Ferrara, and Stotsky (1994, 1999) describes a similar estimation scheme using two auxiliary variables, but is applied for estimation of bounded disturbances. Kolmanovsky, Sivergina, and Sun (2006) incorporates this design for input estimation and derives similar stability results as Stotsky and Kolmanovsky (2002). The proof of estimator stability for the high-gain input observer developed in Stotsky and Kolmanovsky (2002) is also presented in the appendix of this paper, and shows that with sufficiently large observer gain, the estimation error tends to zero with increasing time. This analysis as it stands, while very useful, does have some limitations, which will be detailed in the following sections. Specifically, the stability analysis previously presented in Stotsky and Kolmanovsky (2002) is extended here to provide a less conservative convergence guarantee for the estimator error. A strategy is also outlined for selecting the observer gain based on system dynamics, measurement uncertainty, allowable steady-state error, and desired convergence time.

The estimation scheme, stability analysis, and gain selection strategy are applied to estimate the effective compression ratio (ECR) of a diesel engine. The effective compression ratio is a measure of the effective amount the in-cylinder gas mixture that is compressed above intake manifold conditions and can be varied through modulation of the intake valve closing (IVC) time (He & Durrett, 2008; Modiyani et al., 2011). The effective compression ratio is a key gas exchange and combustion input for targeting advanced combustion events aimed at fuel efficiency, increased torque and reduced emissions (Helmantel, Gustavsson, & Denbratt, 2005; Jia, Xie, Wang, & Peng, 2011; Kulkarni, Stricker, Blum, & Shaver, 2008; Murata et al., 2007, 2008; Nevin, Sun, Manuel, Gonzalez, & Reitz, 2007). Historically, methods for determining the compression ratio of an engine rely on the availability of accurate in-cylinder pressure measurements (Hountalas, Mavropoulos, & Kourbetis, 2005; Klein & Eriksson, 2006; Lamaris & Hountalas, 2009; Watzenig, Steiner, & Sommer, 2008). However, accurate in-cylinder pressure measurements are not commonly available in production engines, motivating the need for a real-time estimation scheme for effective compression ratio using only information available from stock engine sensors. The work presented here builds on the previous work by the

* Corresponding author. Tel.: +1 765 491 6052; fax: +1 765 494 0787.
E-mail address: gshaver@purdue.edu (G.M. Shaver).

0967-0661/$ - see front matter © 2012 Elsevier Ltd. All rights reserved.
http://dx.doi.org/10.1016/j.conengprac.2012.11.009

authors (Stricker, Kocher, Koeberlein, Van Alstine, & Shaver, 2012), in which an estimation scheme was developed for the effective compression ratio relying only on typical production-viable on-engine sensors, including manifold temperatures and pressures, fresh air and exhaust gas flows. In that effort, the estimator gain was selected in an ad hoc manner, and the observer design was not analyzed for stability or robustness. In this paper, the stability and robustness analysis is applied to the ECR estimation application, and the gain selected strategy is employed to determine the gain necessary for desired estimator performance. With this analysis, the estimator will be shown to converge to within one half a compression ratio in under four engine cycles while in the presence of up to 10% measurement uncertainty.

2. Estimator stability, robustness, and convergence rate

2.1. High-gain observer

The high-gain observer design introduced in Stotsky and Kolmanovsky (2002) for a first-order system, Eq. (1), is given by Eqs. (2) and (3)

$$\dot{z} = y + x \tag{1}$$

$$\hat{x} = \kappa z - \varepsilon \tag{2}$$

$$\dot{\varepsilon} = -\kappa\varepsilon + \kappa y + \kappa^2 z \tag{3}$$

where signals z and y are known or measured, x is the unsteady variable to be estimated, κ is the observer gain, and ε is an auxiliary variable. In the case of uncertainty in the variable y, Eq. (3) becomes

$$\dot{\varepsilon} = -\kappa\varepsilon + \kappa y + \kappa\Delta y + \kappa^2 z \tag{4}$$

where Δy is the uncertainty in the variable y. Assuming the unsteady variable x is $B_{1\Delta}$-Lipschitz, the stability result, derived in Stotsky and Kolmanovsky (2002) as well as the appendix, is given by

$$\frac{d(e^2)}{dt} \le -\kappa e^2 + \frac{B_{1\Delta}^2}{\kappa} \tag{5}$$

$$\Rightarrow |e(t)| \le \sqrt{e_0^2 \exp(-\kappa t) + \frac{B_{1\Delta}^2}{\kappa^2}} \tag{6}$$

from Eq. (A.33), where e is the estimation error and $B_{1\Delta}$ is an upper bound on physical system dynamics, given by

$$sup_t |\dot{x} + \kappa\Delta y| \le B_{1\Delta} \tag{7}$$

with a worst-case value for $B_{1\Delta}$ defined as

$$B_{1\Delta} = |\dot{x}|_{max} + \kappa|\Delta y| \tag{8}$$

The transient error bound result of Eq. (6) is illustrated in Fig. 1 with the dashed black line. Note that the error is not guaranteed to converge to zero, per Eq. (6), indicated by the dashed grey line. This result from Stotsky and Kolmanovsky (2002) indicates that the squared error will always be less than this bound, however, it does not necessarily guarantee that the error will always decrease. As an example, the transient error may possibly follow a path indicated by the red line in Fig. 1, where the estimator error might actually initially increase. As such, no guarantee on the convergence rate may be made.

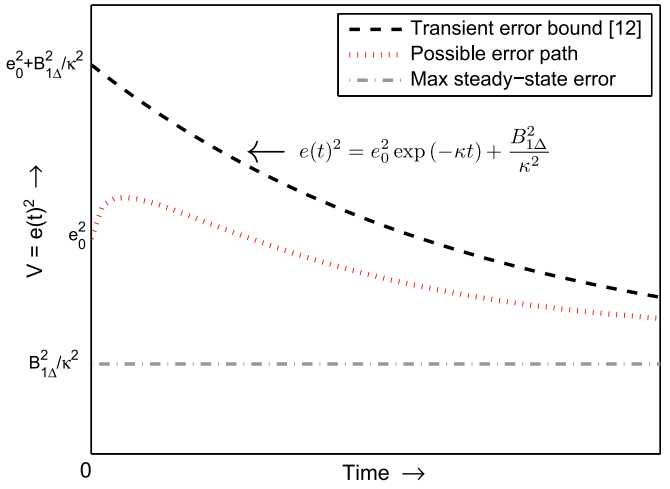

Fig. 1. Transient error bounds. (For interpretation of the references to color in this figure legend, the reader is referred to the web version of this article.)

2.2. Development of a less conservative estimator performance guarantee

Upon further inspection of Eq. (5), with the candidate Lyapunov function V

$$V = e^2 \Rightarrow \dot{V} \le -\kappa V + \frac{B_{1\Delta}^2}{\kappa} \tag{9}$$

make the assumption that

$$-\kappa V + \frac{B_{1\Delta}^2}{\kappa} < 0 \tag{10}$$

which is true as long as

$$\kappa > \frac{B_{1\Delta}}{|e|} \tag{11}$$

In the worst case, corresponding to the slowest rate of decreasing squared error, $\dot{V}$ from Eq. (9) is given by

$$\dot{V}_{max} = -\kappa V + \frac{B_{1\Delta}^2}{\kappa} = -\kappa\left(V - \frac{B_{1\Delta}^2}{\kappa^2}\right) \tag{12}$$

Solving for V_{max}, consider the candidate solution

$$V_{max} = C_1 \exp(-\kappa t) + C_2 \tag{13}$$

where coefficients C_1 and C_2 are solved for using initial conditions:

$$V_{max}(0) = V_0 = C_1 + C_2 \Rightarrow C_2 = V_0 - C_1 \tag{14}$$

$$\dot{V}_{max} = -C_1\kappa \exp(-\kappa t) = -\kappa V + \frac{B_{1\Delta}^2}{\kappa}$$

$$\dot{V}_{max}(0) = -C_1\kappa = -\kappa V(0) + \frac{B_{1\Delta}^2}{\kappa} = -\kappa V_0 + \frac{B_{1\Delta}^2}{\kappa}$$

$$\Rightarrow C_1 = V_0 - \frac{B_{1\Delta}^2}{\kappa^2} \tag{15}$$

$$\Rightarrow C_2 = \frac{B_{1\Delta}^2}{\kappa^2} \tag{16}$$

resulting in the following solution for V_{max}:

$$V_{max} = \left(V_0 - \frac{B_{1\Delta}^2}{\kappa^2}\right)\exp(-\kappa t) + \frac{B_{1\Delta}^2}{\kappa^2} \tag{17}$$

It then follows that, from Eqs. (9) and (12), a new constraint is put on V and $\dot{V}$:

$$\dot{V} \le \dot{V}_{max} = -\kappa\left(V_0 - \frac{B_{1\Delta}^2}{\kappa^2}\right)\exp(-\kappa t) \tag{18}$$

$$V \le V_{max} = \left(V_0 - \frac{B_{1\Delta}^2}{\kappa^2}\right)\exp(-\kappa t) + \frac{B_{1\Delta}^2}{\kappa^2} \tag{19}$$

This new result is illustrated in Fig. 2, where the black dashed line indicates the error bound guaranteed by Stotsky and Kolmanovsky (2002) (Eq. (A.33)), and the blue line indicates the guarantee given in Eq. (19).

Inspecting Eq. (19) further, it is evident that the squared error $V = e^2$ will always decrease when it is larger than $B_{1\Delta}^2/\kappa^2$, the upper bound for the steady-state error. As such, the squared error is constantly decreasing at a rate consistent with a time constant (τ) no larger than $\tau = 1/\kappa$. V_{max} is a new guaranteed upper bound on the transient squared error. In contrast with the previous guarantee from Stotsky and Kolmanovsky (2002), the guarantee given in Eq. (19) is less conservative in regards to both the transient error bound and error convergence, and proves that the error will always be decreasing. As with the previous guarantee from Stotsky and Kolmanovsky (2002), the error converges to the same steady-state error indicated by the grey dashed line in Fig. 2, corresponding to maximum steady-state error $e_{ss,max}^2 = B_{1\Delta}^2/\kappa^2$. The guarantee given in Eq. (19) shows that the transient error will converge to the acceptable error at a rate equal to or faster than that determined by the gain κ.

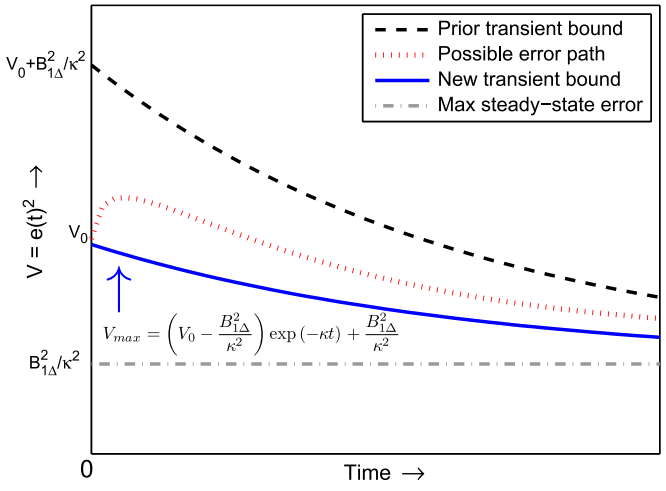

Fig. 2. New transient error bounds. (For interpretation of the references to color in this figure legend, the reader is referred to the web version of this article.)

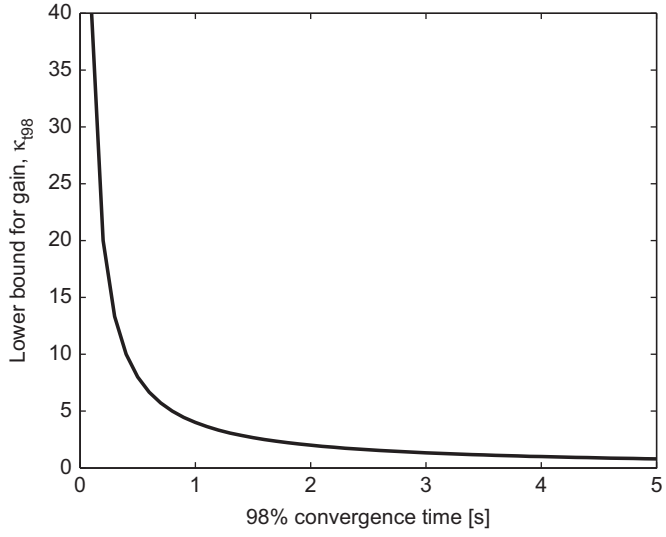

Fig. 3. Observer gain vs desired convergence time.

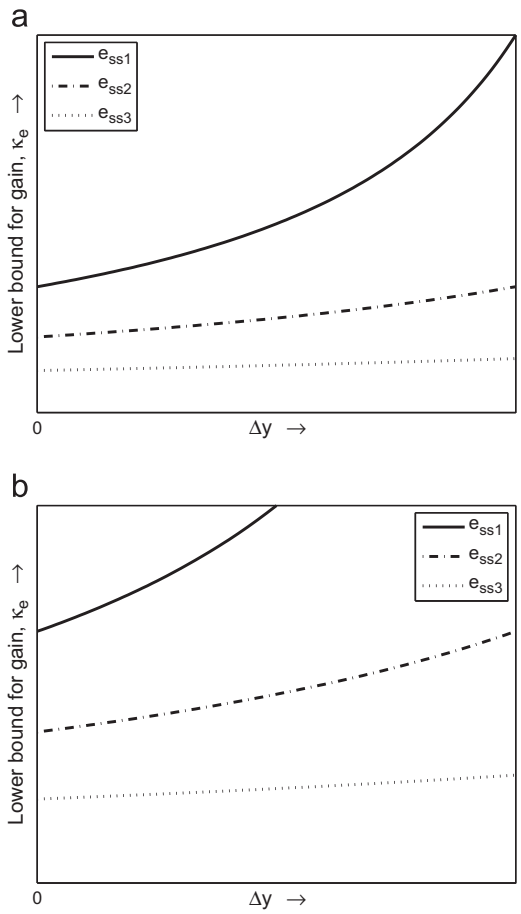

Fig. 4. Example of gain trade-off: (a) low $|\dot{x}|_{max}$ and (b) higher $|\dot{x}|_{max}$.

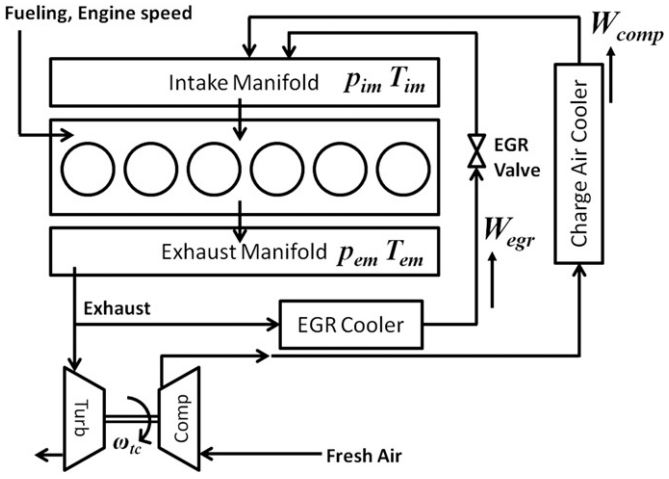

Fig. 5. Engine schematic.

3. Selection of observer gain

The result of the stability proof in Stotsky and Kolmanovsky (2002), Eq. (6), intuitively suggests that a large observer gain, κ, is necessary to drive the estimated quantity close to the true value, but does not clearly indicate how to intelligently select an appropriate gain. On the other hand, the result in the previous section, given by Eqs. (18) and (19), provide an opportunity to select the gain in a straightforward way. There are four factors that will direct the choice of the gain value, including the (1) convergence time, t_{98}, when the estimator reaches 98% of the final steady-state value, (2) uncertainty in the measurement of the variable y, Δy, (3) maximum rate of change, $|\dot{x}|_{max}$, of the unsteady variable x to be estimated, and (4) allowable steady-state estimation error. Based on these four factors, two lower bounds for the observer gain will be derived, denoted $\kappa_{t_{98}}$ (based on convergence time) and κ_e (based on measurement uncertainty, system dynamics, and acceptable steady-state error). Ultimately, the gain chosen should satisfy

$$\kappa = \max(\kappa_{t_{98}}, \kappa_e) \tag{20}$$

as selecting the larger of the two gains will automatically satisfy constraints defined by all three of the contributing factors, each of which will be outlined in the following sections.

Table 1
ECR estimator inputs and constants.

Inputs		Constants	
W_{egr}	EGR flow (kg/min)	k	1.35
T_{egr}	EGR gas temperature (K)	c_p	1.005
W_{comp}	Fresh air flow (kg/min)	c_v	0.7179
T_{cac}	CAC outlet temperature (K)	R_{im}	0.287
p_{im}	Intake pressure (kPa)	γ_{im}	1.3994
T_{im}	Intake temperature (K)	V_{tdc}	4.1297e−4 m^3
p_{em}	Exhaust pressure (kPa)	V_d	0.067 m^3
T_{clt}	Coolant temperature (K)	V_{ivo}	6.9530e−4 m^3
IVO	Intake valve open time (CAD)	V_{im}	0.04 m^3
IVC	Intake valve close time (CAD)	V_{evc}	9.9703e−4 m^3
EVC	Exhaust valve close time (CAD)		
N	Engine speed (rpm)		

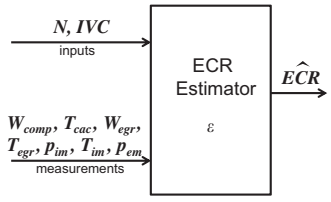

Fig. 6. Estimation scheme block diagram.

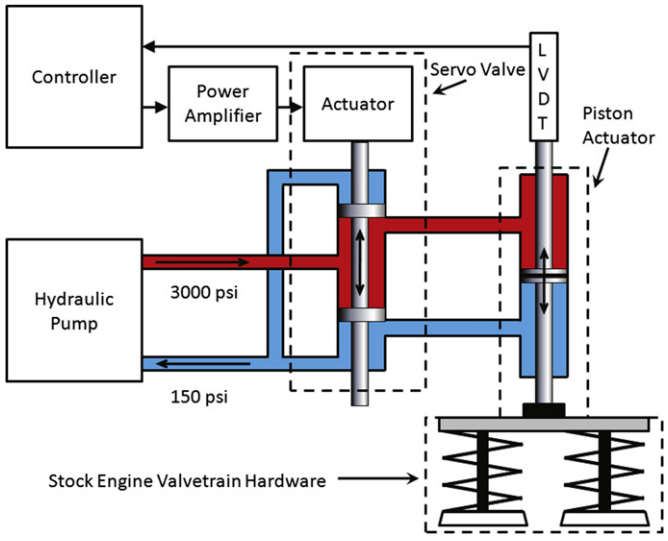

Fig. 7. Schematic of variable valve actuation system.

3.1. Convergence time

In order to be a useful control signal, the estimator error must converge in a reasonable amount of time. Here, estimator convergence is considered to occur when the estimator reaches 98% of the final steady-state value, equal to four time constants, and by inspection of Eq. (19), a guaranteed convergence time can be defined as

$$t_{98} = 4\tau = \frac{4}{\kappa} \tag{21}$$

Table 2
Observer gain selection for convergence time.

Speed (rpm)	$n=2$	$n=4$	$n=6$	$n=8$	$n=10$
2300	16.667	8.333	5.556	4.167	3.333
1850	20	10	6.667	5	4
1000	25	12.5	8.333	6.25	5
1200	30.833	15.417	10.278	7.708	6.167
1500	38.333	19.167	12.778	9.583	7.667

Table 3
Engine operating points.

Case	Speed (rpm)	Torque (ft lbs)
1	2300	385
2	1850	300
3	1000	150
4	1200	400
5	1500	450

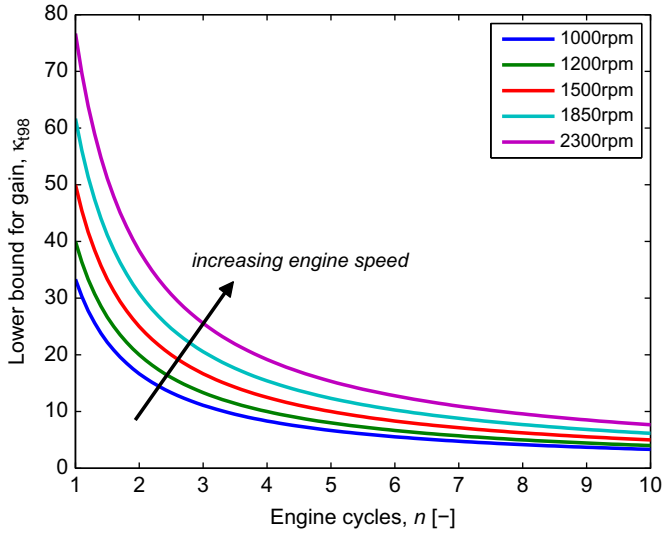

Fig. 8. Relationship between gain and convergence time.

which subsequently defines a lower limit for the observer gain:

$$\kappa_{t_{98}} \geq \frac{4}{t_{98}} \tag{22}$$

This relationship between the observer gain and convergence time is illustrated in Fig. 3, which demonstrates that larger gains are needed for shorter convergence times.

3.2. Measurement uncertainty, steady-state estimation error

A second major factor to consider when selecting a gain is the uncertainty in measurements. Recall from Eqs. (10) and (12), for estimator stability, $\dot{V}$ must be negative definite

$$\dot{V} \leq -\kappa V + \frac{B_{1\Delta}^2}{\kappa} < 0 \tag{23}$$

and the following bound was put on the observer gain, κ, from Eq. (11):

$$\kappa > \frac{B_{1\Delta}}{|e|} \tag{24}$$

where, from Eq. (8), in the worst case, $B_{1\Delta}$ may be defined as

$$B_{1\Delta} = |\dot{x}|_{max} + \kappa|\Delta y| \tag{25}$$

The constraint on the observer gain then becomes

$$\kappa_e > \frac{|\dot{x}|_{max}}{|e| - |\Delta y|} \tag{26}$$

From this equation, the impact of the third and fourth contributing factors, system dynamics (i.e. $|\dot{x}|_{max}$) and the acceptable steady-state error e, is also evident, and Fig. 4(a) illustrates the relationship between the allowable steady-state error, the measurement uncertainty, and the lower bound on the observer gain. Each curve represents a different steady-state error, with

$$e_{ss1} < e_{ss2} < e_{ss3} \tag{27}$$

Each e_{ss} curve demonstrates the trade-off between measurement uncertainty, Δy, and the required observer gain. For handling larger uncertainties, larger gains are needed. Likewise, a larger gain is needed when the estimator must perform with smaller error. If there is a larger upper bound on $|\dot{x}|_{max}$, the curves also shift to higher gains, as shown in Fig. 4(b). Returning to Eq. (20), and based on the four factors discussed, the observer gain is chosen to satisfy the following:

$$\kappa = \max\left(\kappa_{t_{98}} \geq \frac{4}{t_{98}}, \kappa_e > \frac{|\dot{x}|_{max}}{|e_{ss}| - |\Delta y|}\right) \tag{28}$$

This method of determining a lower bound for the observer gain, κ, based on the four factors mentioned, is an analysis that, to the author's knowledge, has not been seen before for this particular high-gain estimation strategy.

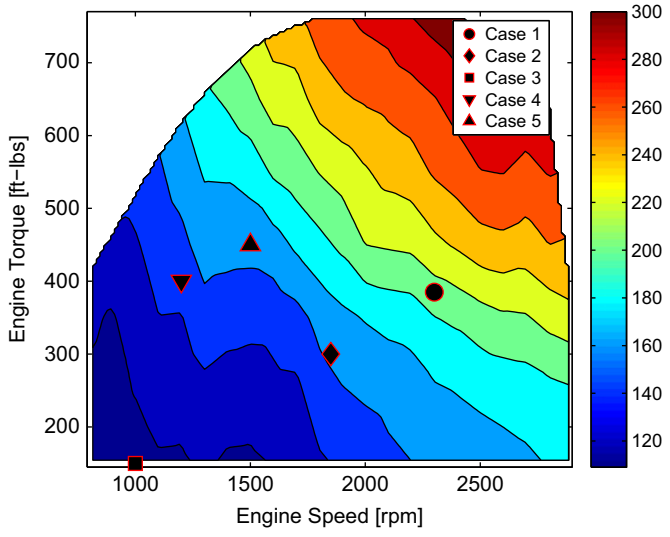

Fig. 9. Intake manifold pressure. (For interpretation of the references to color in this figure legend, the reader is referred to the web version of this article.)

4. Application to ECR estimation in diesel engines with flexible intake valve actuation

In a prior effort (Stricker et al., 2012), the author utilized the high-gain observer (Eqs. (2) and (3)) to estimate the effective compression ratio of a diesel engine that uses flexible intake valve actuation, a schematic of which is shown in Fig. 5. In that effort, the estimator gain was selected in an ad hoc manner. In contrast, the following sections will demonstrate the use of the gain selection methodology outlined in Section 3. An additional difference with the prior effort (Stricker et al., 2012) is that the

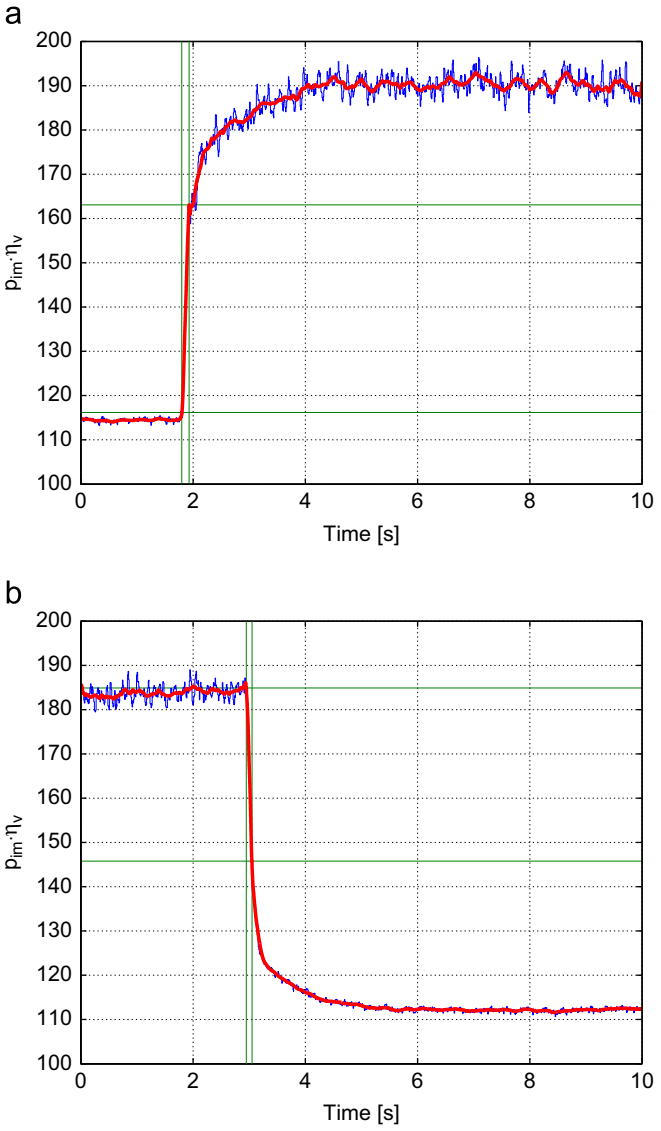

Fig. 10. System dynamics for Case 1: (a) Jump 1 and (b) Jump 2. (For interpretation of the references to color in this figure legend, the reader is referred to the web version of this article.)

estimator error convergence guarantees per Eq. (19) will be compared to, and shown to be consistent with, the experimental data.

4.1. High-gain observer applied to ECR estimation

The ECR estimation scheme uses intake manifold pressure dynamics, given by

$$\dot{p}_{im} = \frac{\gamma_{im} R_{im}}{V_{im}} (W_{egr} T_{egr} + W_{comp} T_{cac} - W_e T_{im}) \tag{29}$$

here W_{comp} and T_{cac} are the measured values of fresh air flow through the compressor and the gas temperature of the fresh air at the charge air cooler outlet (see Fig. 5). Exhaust gas recirculation (EGR) flow, W_{egr}, is determined using manifold pressures and standard orifice flow equations, and T_{egr} is the temperature of the recirculated exhaust gases. R_{im} and γ_{im} are the gas constant and ratio of specific heats of the air in the intake manifold, respectively, both taken at ambient conditions. V_{im} is the volume of the intake manifold, considered to be the volume between the compressor outlet and the cylinders. T_{im} is the temperature in the intake manifold.

Charge flow, W_e, can be described by the speed-density equation (Heywood, 1988):

$$W_e = \frac{1}{2} \rho_{im} \eta_v V_d N \tag{30}$$

where V_d is the displacement volume of the engine, N is the engine speed in revolutions per minute, and η_v is the volumetric efficiency. The gas density in the intake manifold, ρ_{im}, can be written in terms of intake manifold temperature and pressure via the ideal gas law. Charge flow is then written as

$$W_e = \frac{p_{im}}{2 R_{im} T_{im}} \eta_v V_d N \tag{31}$$

and the p_{im} dynamic equation (Eq. (29)) can be written as

$$\dot{p}_{im} = \frac{\gamma_{im} R_{im}}{V_{im}} (W_{egr} T_{egr} + W_{comp} T_{cac}) - \frac{\gamma_{im} p_{im}}{2 V_{im}} \eta_v V_d N \tag{32}$$

z, y and x are chosen as follows:

$$z = p_{im} \tag{33}$$

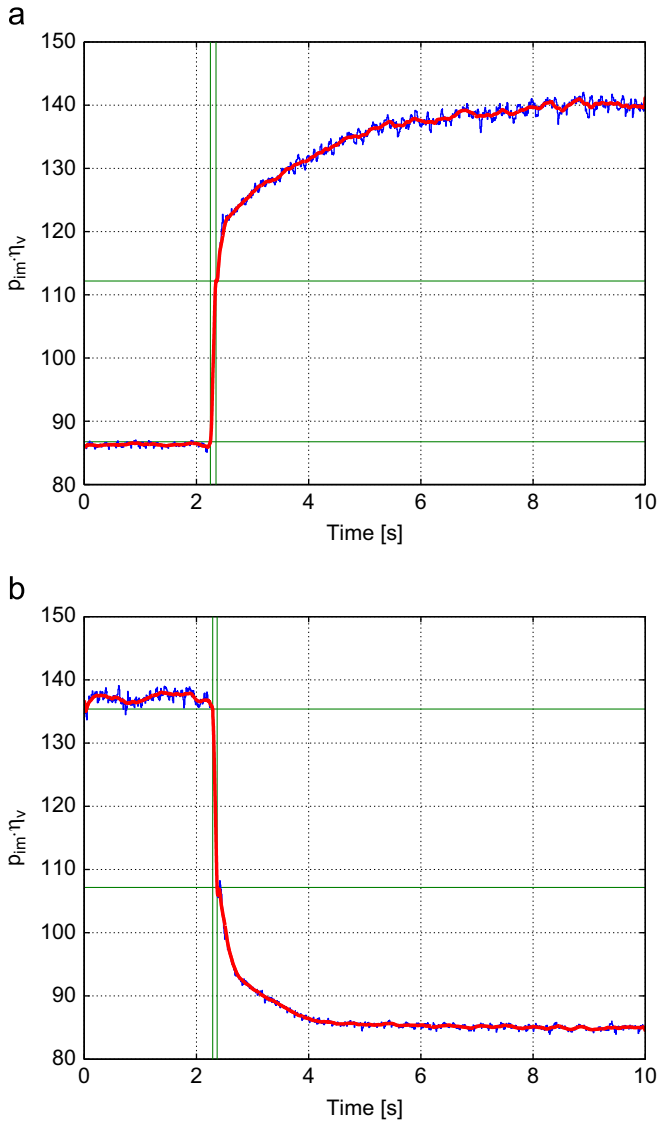

Fig. 11. System dynamics for Case 2: (a) Jump 1 and (b) Jump 2. (For interpretation of the references to color in this figure legend, the reader is referred to the web version of this article.)

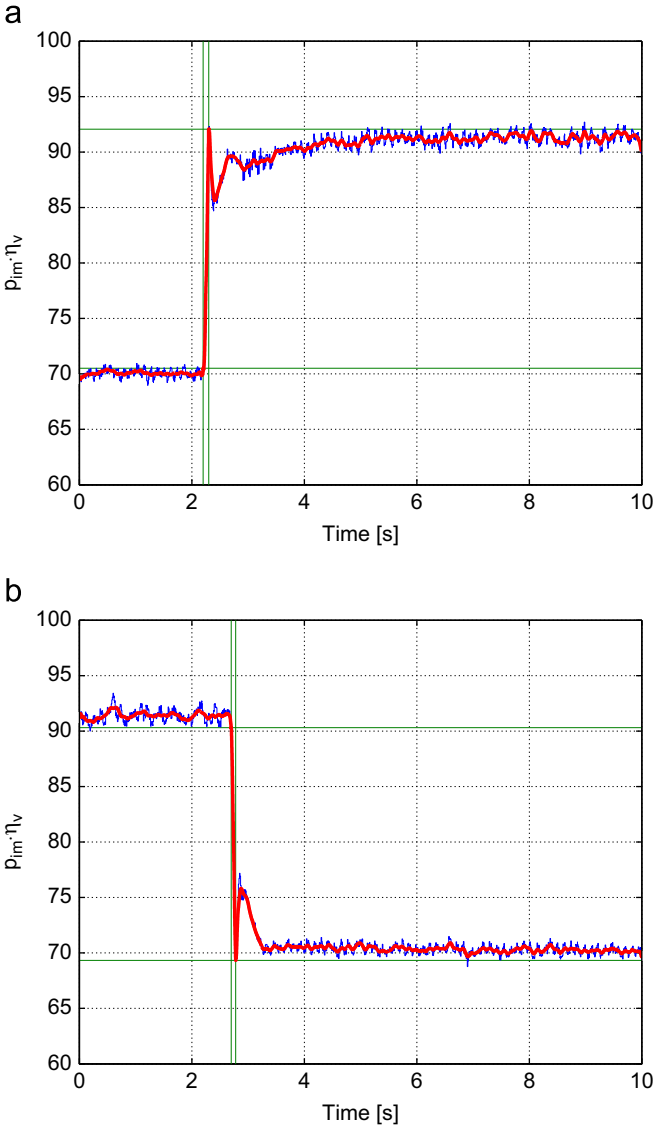

Fig. 12. System dynamics for Case 3: (a) Jump 1 and (b) Jump 2. (For interpretation of the references to color in this figure legend, the reader is referred to the web version of this article.)

$$y = \frac{\gamma_{im} R_{im}}{V_{im}} (W_{egr} T_{egr} + W_{comp} T_{cac}) \tag{34}$$

$$x = -\frac{\gamma_{im} p_{im}}{2V_{im}} \eta_v V_d N \tag{35}$$

With these assignments, it is seen that Eq. (32) becomes exactly the first-order system described by Eq. (1). Eqs. (1) and (2) are combined with Eqs. (3) and (33)–(35) to arrive at an estimate for η_v:

$$\hat{\eta}_v = \frac{2V_{im}(\varepsilon - \kappa p_{im})}{\gamma_{im} p_{im} V_d N} \tag{36}$$

with ε dynamics given by:

$$\dot{\varepsilon} = \kappa^2 p_{im} - \kappa\varepsilon + \kappa \frac{\gamma_{im} R_{im}}{V_{im}} (W_{egr} T_{egr} + W_{comp} T_{cac}) \tag{37}$$

A physically based volumetric efficiency model previously developed in Kocher, Koeberlein, Van Alstine, Stricker, and Shaver (2011) is then employed to calculate the effective compression ratio, ECR. This model is given as follows:

$$\eta_v = \frac{p_{im}\left(\frac{V_{tdc} \cdot ECR}{V_{ivc}}\right)^k V_{ivc} \frac{c_v}{R} - p_{em} V_{ivo} \frac{c_v}{R} - p_{em}(V_{evc} - V_{ivo}) \frac{c_p}{R}}{p_{im} V_d \frac{c_p}{R}} + \frac{p_{im}(V_{tdc} \cdot ECR - V_{ivo}) + \frac{ht}{1000}(T_{wall} - T_{im})(SA)}{p_{im} V_d \frac{c_p}{R}} \tag{38}$$

In the above equation, V_{ivo}, V_{evc} and V_{ivc} are the respective in-cylinder combustion chamber volumes at the time the intake valve opens, the time the exhaust valve opens, and the time the intake valve closes, respectively. V_{tdc} is the in-cylinder volume

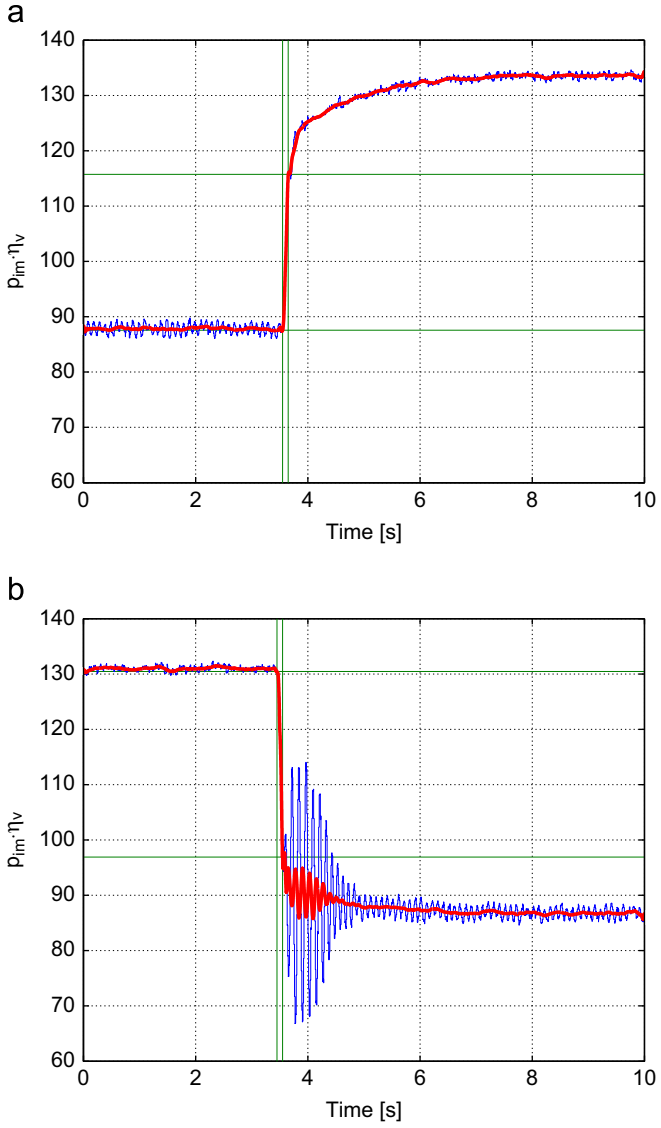

Fig. 13. System dynamics for Case 4: (a) Jump 1 and (b) Jump 2. (For interpretation of the references to color in this figure legend, the reader is referred to the web version of this article.)

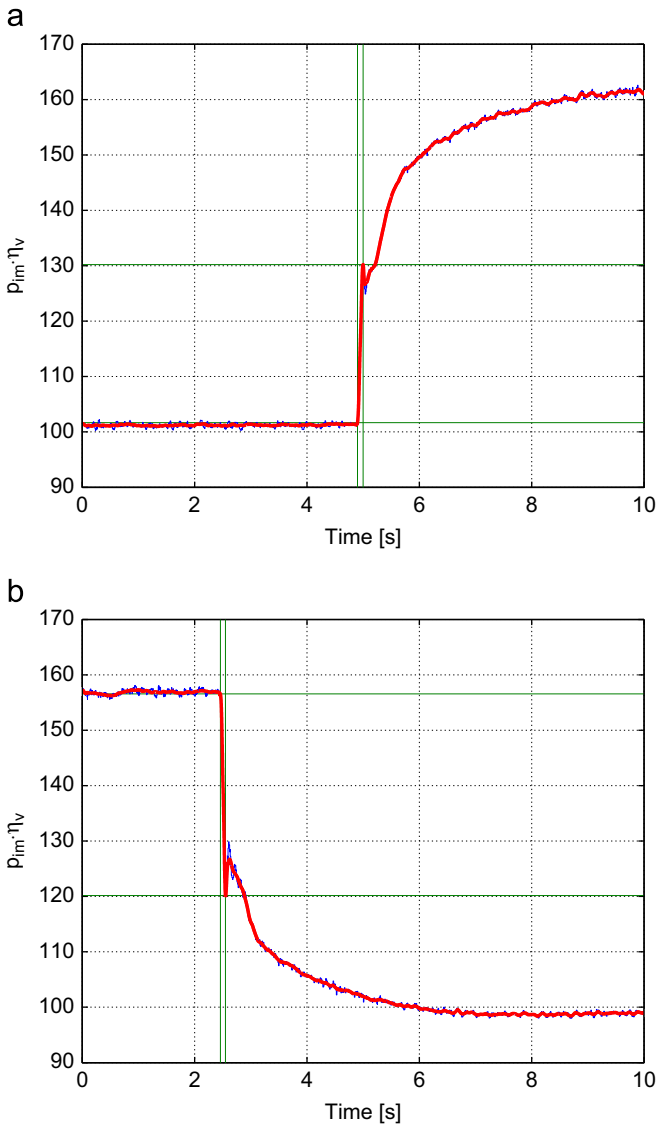

Fig. 14. System dynamics for Case 5: (a) Jump 1 and (b) Jump 2. (For interpretation of the references to color in this figure legend, the reader is referred to the web version of this article.)

Table 4
ECR timing and transient test nomenclature.

Name	IVC time (CAD)	Test	Step change from
IVC1	510	Jump 1	IVC1 to IVC2
IVC2	565 (nominal)	Jump 2	IVC2 to IVC1

when the piston reaches top-dead-center. c_p, c_v and R are specific heats and gas constant of the gas in the intake manifold, and p_{em} is the exhaust manifold pressure, a stock measurement typically found on production diesel engines. The polytropic compression coefficient, k, is taken to be 1.35, a typical value for direct-injection diesel engines (Heywood, 1988). The heat transfer coefficient, ht, is a function of engine speed (N), intake manifold temperature and pressure (T_{im}, p_{im}). SA is the integrated surface area, and is a function of intake valve open and close time (IVO, IVC), exhaust valve close time (EVC), and engine speed. The temperature of the cylinder walls, T_{wall} is taken as the average of the exhaust temperature (T_{em}) and the engine coolant temperature (T_{clt}).

Once an estimate of volumetric efficiency is obtained via Eq. (36), the effective compression ratio is solved for numerically using the model given in Eq. (38). Estimator inputs and constants are listed in Table 1, as well as shown in a block diagram of the estimation scheme in Fig. 6. As shown, the ECR estimation scheme does not require in-cylinder pressure data and uses only measurements readily available on production engines. The overall estimation scheme is given by solving Eqs. (36)–(38) for $\hat{ECR}$.

Table 5
Observer gain selection.

Case	Min. p_{im} (kPa)	Test	$\left\|\frac{d}{dt}(p_{im}\eta_v)\right\|$ (kPa/s)	κ_e	$\kappa_{t_{98}}$	κ
1	185	Jump 1	361.6	110.163	8.333	111
		Jump 2	391.4	73.453		74
2	135	Jump 1	254.3	80.277	10	81
		Jump 2	352.7	96.140		97
3	100	Jump 1	215.5	103.841	12.5	104
		Jump 2	262.3	111.356		112
4	130	Jump 1	281.8	64.271	15.417	65
		Jump 2	335.5	86.805		87
5	150	Jump 1	285.3	70.131	19.167	71
		Jump 2	404.5	92.365		93

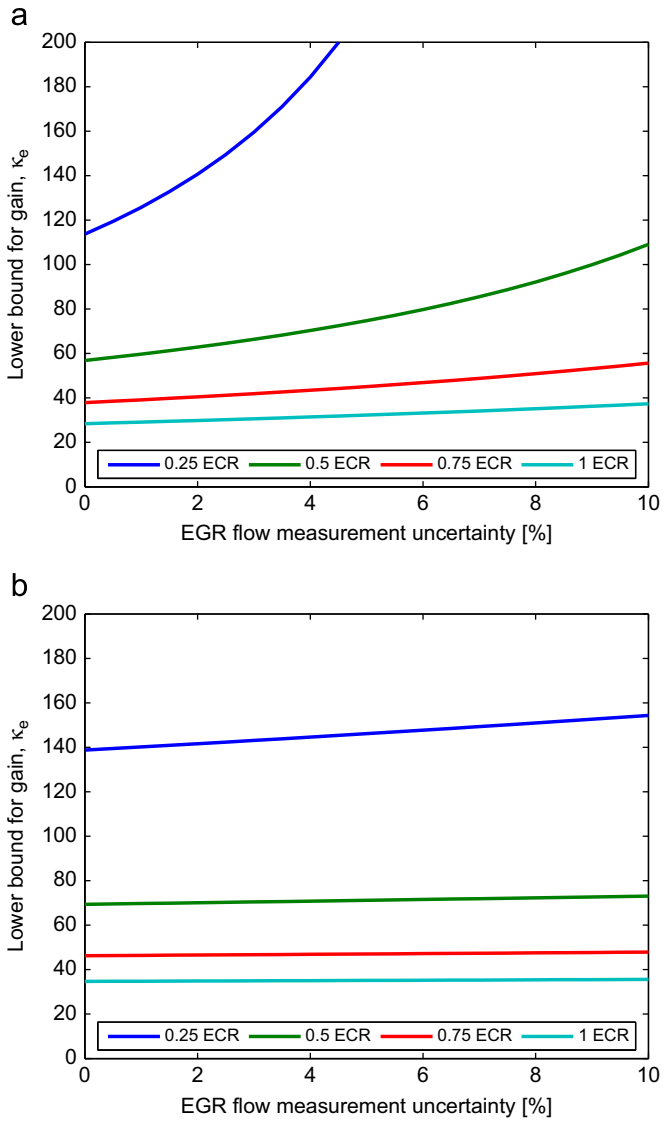

Fig. 15. Uncertainty, convergence, ECR trade-off for Case 1: (a) ECR ≈ 18 and (b) ECR ≈ 13. (For interpretation of the references to color in this figure legend, the reader is referred to the web version of this article.)

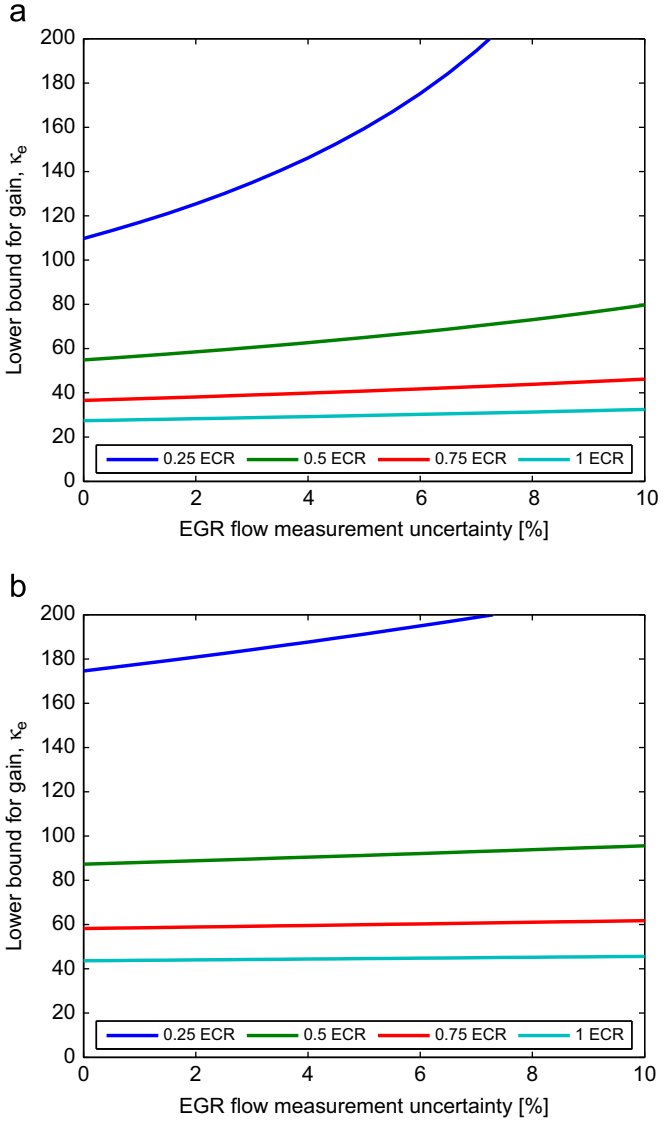

Fig. 16. Uncertainty, convergence, ECR trade-off for Case 2: (a) ECR ≈ 18 and (b) ECR ≈ 14. (For interpretation of the references to color in this figure legend, the reader is referred to the web version of this article.)

5. Gain selection for ECR estimation

As noted previously, in Stricker et al. (2012) the estimator gain had been selected via a "trial and error" strategy. In this section, the gain is determined systematically via the gain selection strategy presented in Section 3, following a short description of the engine test bed.

5.1. Engine test bed

The experimental engine used to demonstrate the ECR estimation and gain selection strategies is a 2008 Cummins ISB engine, a schematic of which is shown in Fig. 5. The engine is a 6.7 L, 350 horsepower, in-line 6-cylinder direct-injection diesel engine with a 17.3:1 geometric compression ratio. The engine cylinder head has a 4-valve design, with two exhaust and two intake valves per cylinder. The engine is also outfitted with a Bosch common rail fuel injection system with multi-pulse injection capability, a variable-geometry turbocharger and cooled exhaust gas recirculation with an electronic EGR valve for control of fresh charge and EGR flow to the cylinder. Pressure measurements in the EGR loop and standard orifice equations are used to determine EGR flow on-engine, denoted by W_{egr} in Fig. 5. The engine additionally has stock sensors for intake and exhaust manifold pressures, used as inputs to the estimation scheme.

CO_2 measurements in the intake and exhaust manifolds via fast Cambustion CO/CO_2 emissions analyzers are also used with fresh air flow via a laminar flow element (LFE) to determine a lab-grade measurement of total charge flow ($W_{comp}+W_{egr}$). The LFE measurement of fresh air flow through the compressor and charge air cooler (W_{comp}) effectively emulates a mass air flow (MAF) sensor. A water-cooled in-cylinder pressure transducer is also installed in the engine for cylinder pressure measurements, from which the engine ECR data is calculated using the pressure-based method described in Stricker et al. (2012), and is compared to results from the ECR estimator. Using a dSpace data acquisition system, engine data is sampled at 5 kHz, or every 0.2 ms, and the ECR estimation scheme is implemented using this sampled engine data.

The engine is also equipped with a fully flexible variable valve actuation (VVA) system, manufactured by Team Corporation.

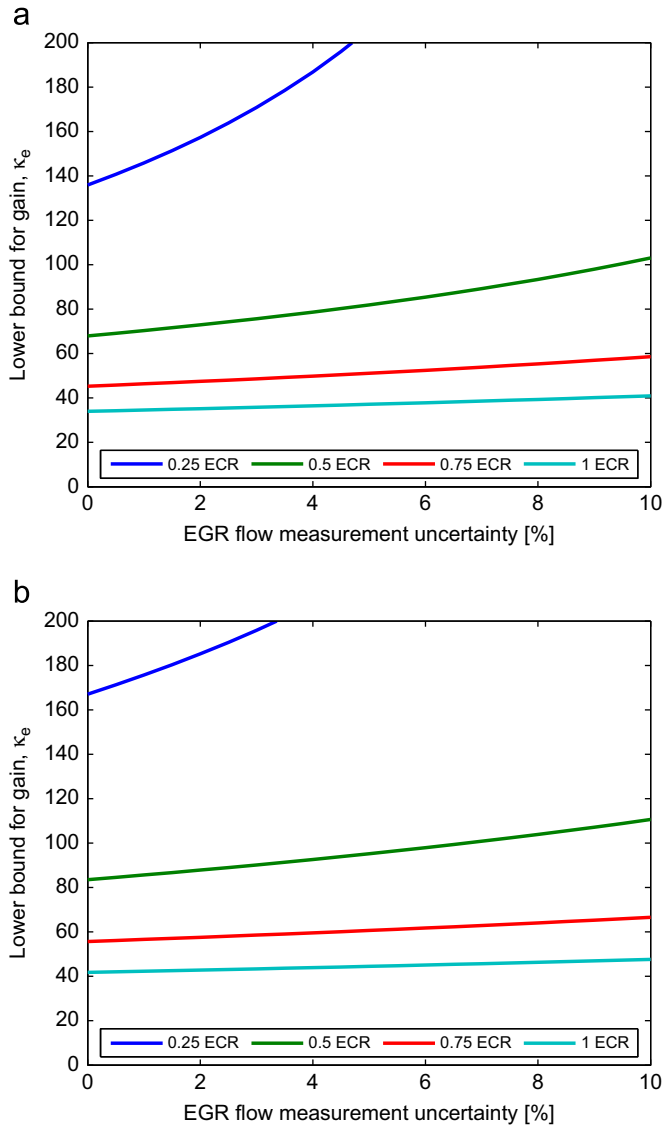

Fig. 17. Uncertainty, convergence, ECR trade-off for Case 3: (a) ECR ≈ 18 and (b) ECR ≈ 14. (For interpretation of the references to color in this figure legend, the reader is referred to the web version of this article.)

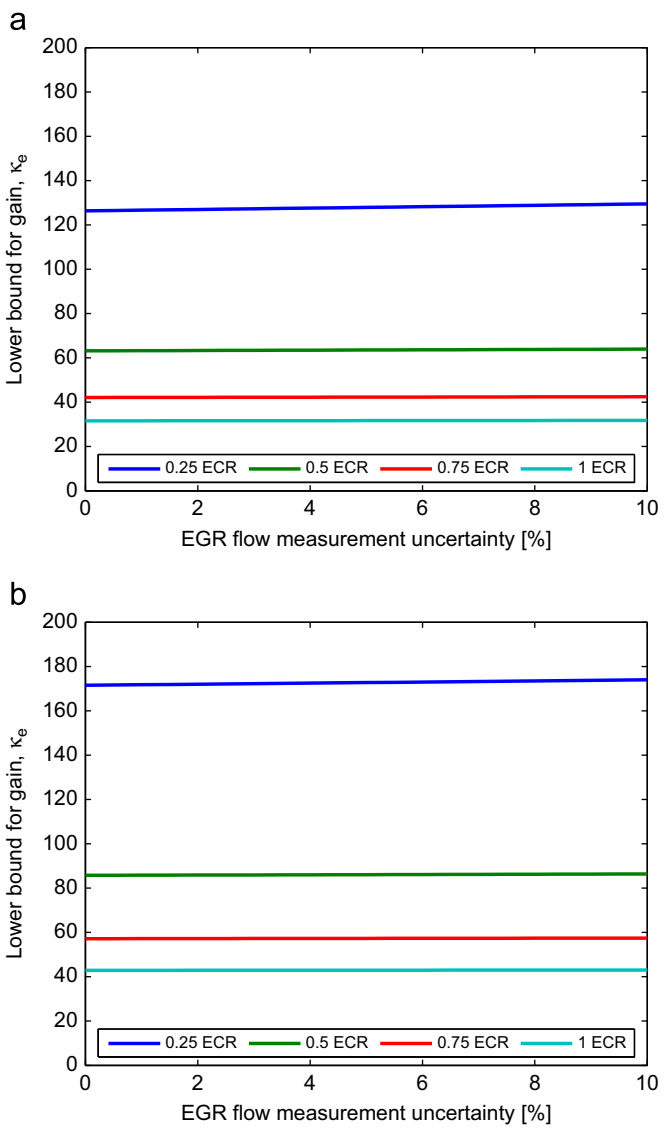

Fig. 18. Uncertainty, convergence, ECR trade-off for Case 4: (a) ECR ≈ 18 and (b) ECR ≈ 14. (For interpretation of the references to color in this figure legend, the reader is referred to the web version of this article.)

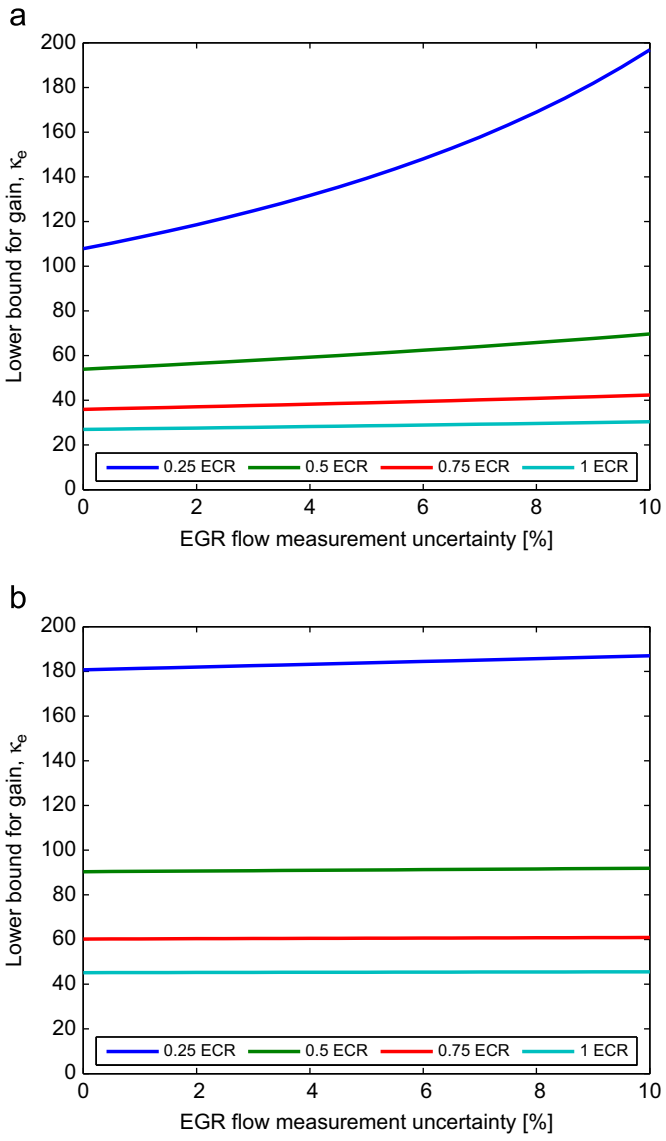

Fig. 19. Uncertainty, convergence, ECR trade-off for Case 5: (a) ECR ≈ 18 and (b) ECR ≈ 14. (For interpretation of the references to color in this figure legend, the reader is referred to the web version of this article.)

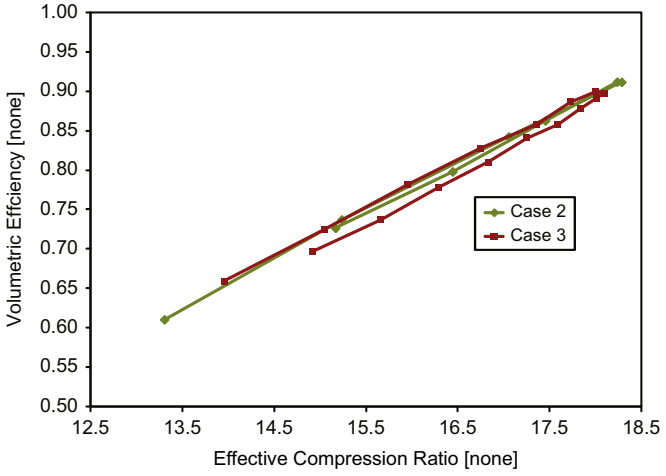

Fig. 20. Relationship between volumetric efficiency and ECR.

The VVA system adds the capability to modify valve events, including opening and closing times, lifts, and ramp rates, on a cylinder-independent, cycle-to-cycle basis. In this study, the VVA system is used to actuate pairs of intake valves; the exhaust valves remain cam-driven in the conventional manner. A basic schematic of the VVA system is shown in Fig. 7, and is operated as follows. A hydraulic power supply sends high pressure hydraulic oil to a servo valve, which shuttles the oil to one side of a piston actuator, which in turn presses on an intake valve crosshead connecting a pair of intake valves. Depending on which side of the piston actuator the high pressure oil is on, the actuator moves up or down, opening and closing the pair of intake valves.

For this application, five operating conditions, listed in Tables 2 and 3, were chosen to illustrate the gain-selection process and estimator convergence results. These operating conditions are characteristic of those typically seen in practice for the engine described in this section. In addition, the estimator gain selection and convergence analysis strategies are generalizable, and as such can be applied to any engine operating condition.

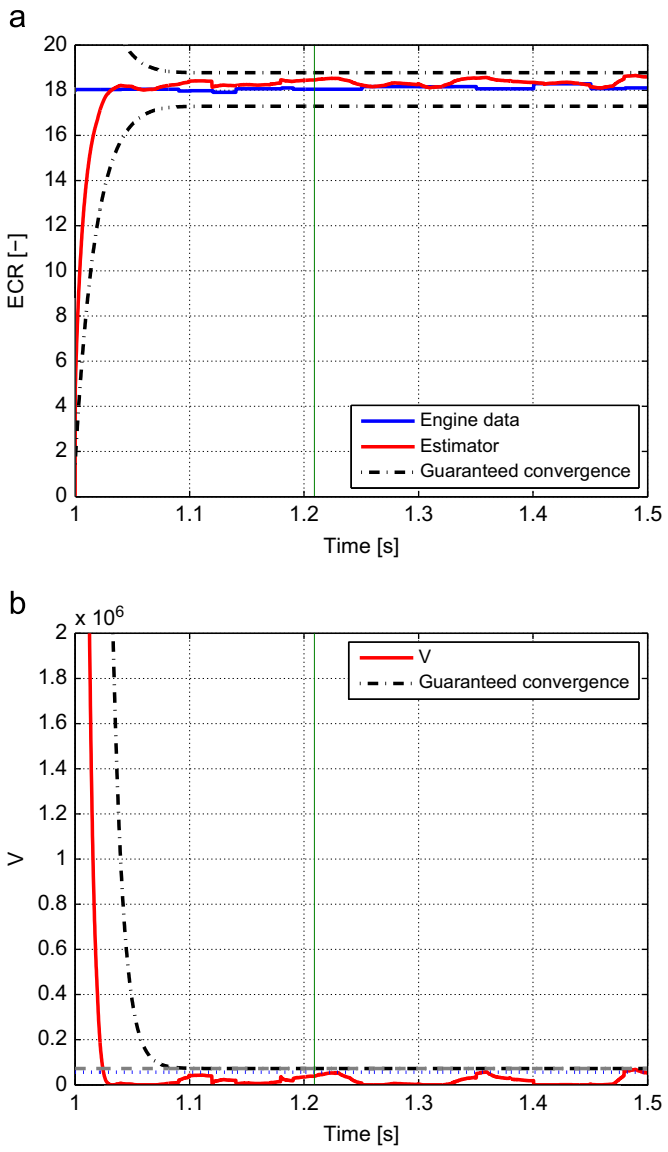

Fig. 21. Estimator convergence for Case 1: ECR ≈ 18. (a) ECR convergence and (b) squared error convergence. (For interpretation of the references to color in this figure legend, the reader is referred to the web version of this article.)

5.2. Convergence time requirements for gain selection

When estimating the effective compression ratio, the observer error is desired to converge within a certain number of engine cycles, n, to be useful for closed-loop control. From Eq. (21), the convergence time for this application is further defined as

$$t_{98} = n \text{ cycles} \cdot \frac{2 \text{ rev}}{\text{cycle}} \cdot \frac{\text{min}}{N \text{ rev}} \frac{60 \text{ s}}{\text{min}} = \frac{120n}{N} \text{s} \tag{39}$$

where N is the engine speed in revolutions per minute. When combined with Eq. (22), this results in the following gain constraint:

$$\kappa_{t_{98}} \geq \frac{4N}{120n} \tag{40}$$

This relationship between the observer gain and convergence time, similar to that in Fig. 3, is shown in Fig. 8. Intuitively, shorter convergence times require higher observer gains, and the gains increase with increasing engine speed, as the time to complete an engine cycle (and hence time for convergence) reduces with higher engine speeds. Table 2 lists observer gains calculated via Eq. (40) for 98% convergence within a selected number of engine cycles, n.

5.3. Error and uncertainty effects on gain selection

Table 1 includes a list of all sensor measurements used as inputs to the estimation scheme. While each sensor inherently has some uncertainty due to tolerance and noise, the largest amount of uncertainty present in this application is from the EGR flow measurement. As in practice, EGR flow is actually a calculation using pressure measurements in the EGR loop and standard orifice equations. This model uncertainty tends to outweigh the parametric uncertainties in relation to sensor tolerance and noise. Hence, for this study, EGR flow uncertainty was selected as the focus of this section. As such, the intake manifold pressure dynamics from Eq. (32) become

$$\dot{p}_{im} = \frac{\gamma_{im} R_{im}}{V_{im}} ((W_{egr} + \Delta W_{egr}) T_{egr} + W_{comp} T_{cac}) - \frac{\gamma_{im} p_{im}}{2V_{im}} \eta_v V_d N \tag{41}$$

where W_{egr} is the true value for EGR flow and ΔW_{egr} is the uncertainty in the measurement of EGR flow. Eq. (34) then

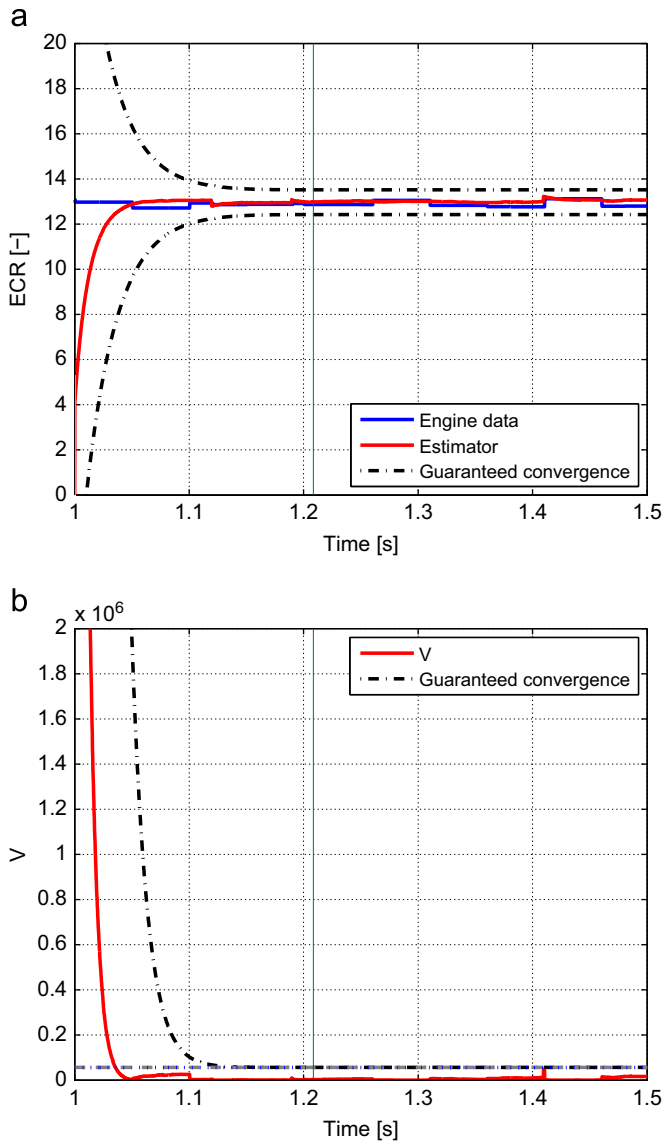

Fig. 22. Estimator convergence for Case 1: ECR ≈ 13. (a) ECR convergence and (b) squared error convergence. (For interpretation of the references to color in this figure legend, the reader is referred to the web version of this article.)

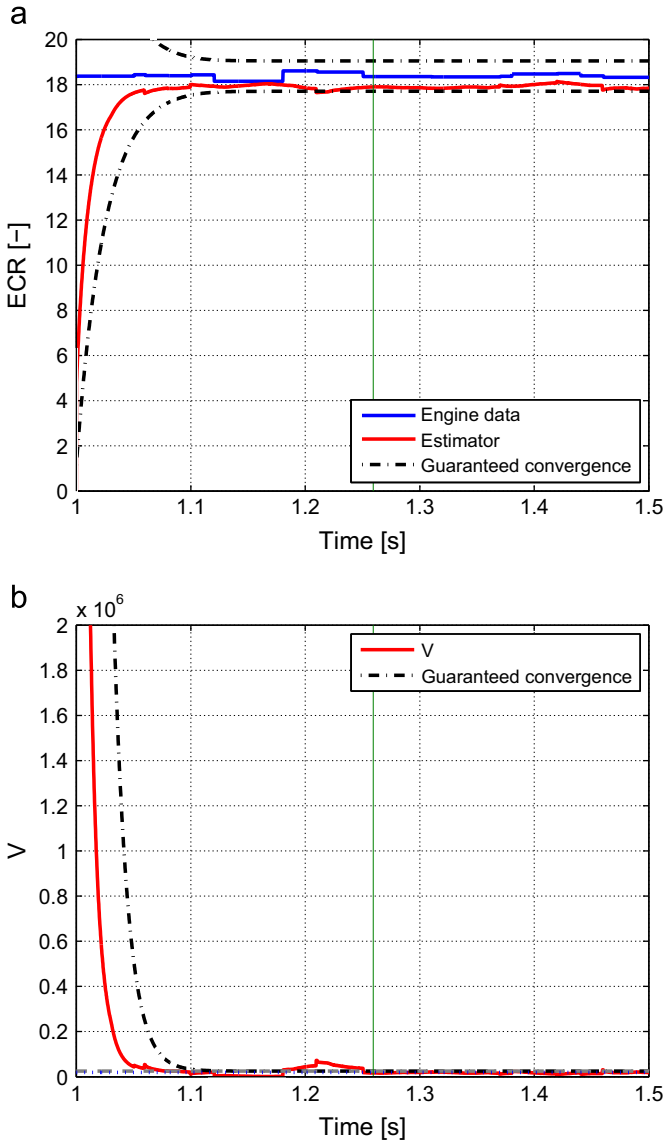

Fig. 23. Estimator convergence for Case 2: ECR ≈ 18. (a) ECR convergence and (b) squared error convergence. (For interpretation of the references to color in this figure legend, the reader is referred to the web version of this article.)

becomes

$$y+\Delta y=\frac{\gamma_{im}R_{im}}{V_{im}}((W_{egr}+\Delta W_{egr})T_{egr}+W_{comp}T_{cac}) \tag{42}$$

By inspection of Eqs. (33), (35), and (42), $|\dot{x}|_{max}$, $|e|$, and Δy in Eq. (26) are given by:

$$|\dot{x}|_{max}=sup_t\left|\frac{d}{dt}\left(-\frac{\gamma_{im}p_{im}}{2V_{im}}\eta_v V_d N\right)\right| \tag{43}$$

$$|e|=\left|(\eta_v-\hat{\eta}_v)\frac{\gamma_{im}V_d N}{2V_{im}}p_{im}\right| \tag{44}$$

$$\Delta y=\frac{\gamma_{im}R_{im}T_{egr}}{V_{im}}\Delta W_{egr} \tag{45}$$

Substituting these into Eq. (26):

$$\kappa_e>\frac{sup_t\left|\frac{d}{dt}\left(-\frac{\gamma_{im}p_{im}}{2V_{im}}\eta_v V_d N\right)\right|}{\left|(\eta_v-\hat{\eta}_v)\frac{\gamma_{im}V_d N}{2V_{im}}p_{im}\right|-\left|\frac{\gamma_{im}R_{im}}{V_{im}}\Delta(W_{egr}T_{egr})\right|} \tag{46}$$

For the system under consideration, intake manifold parameters (V_{im} and γ_{im}) and displacement volume (V_d) are positive constants, and engine speed (N) is slowly varying, so that Eq. (46) reduces to:

$$\kappa_e>\frac{sup_t\left|\frac{d}{dt}(p_{im}\eta_v)\right|}{\left|p_{im}(\eta_v-\hat{\eta}_v)\right|-\left|\frac{2R_{im}}{V_d N}\right|\Delta(W_{egr}T_{egr})|} \tag{47}$$

Fig. 9 displays the steady-state intake manifold pressure conditions for each of the operating points, listed also in Table 3, while Figs. 10–14 show the transient tests carried out, per Table 4, with a smoothed data line plotted in red. The boxed area indicated by the green boundary lines corresponds to the region considered when calculating values of $\dot{x}$. Table 5 also lists the upper bound on $\dot{x}$ for each test and operating condition.

Figs. 15–19 demonstrate the trade-off between error, uncertainty in EGR flow measurement, and required gain for this particular application. Each curve indicates a desired error tolerance in the estimation of effective compression ratio. Blue lines, for example, illustrates the relationship between the gain needed

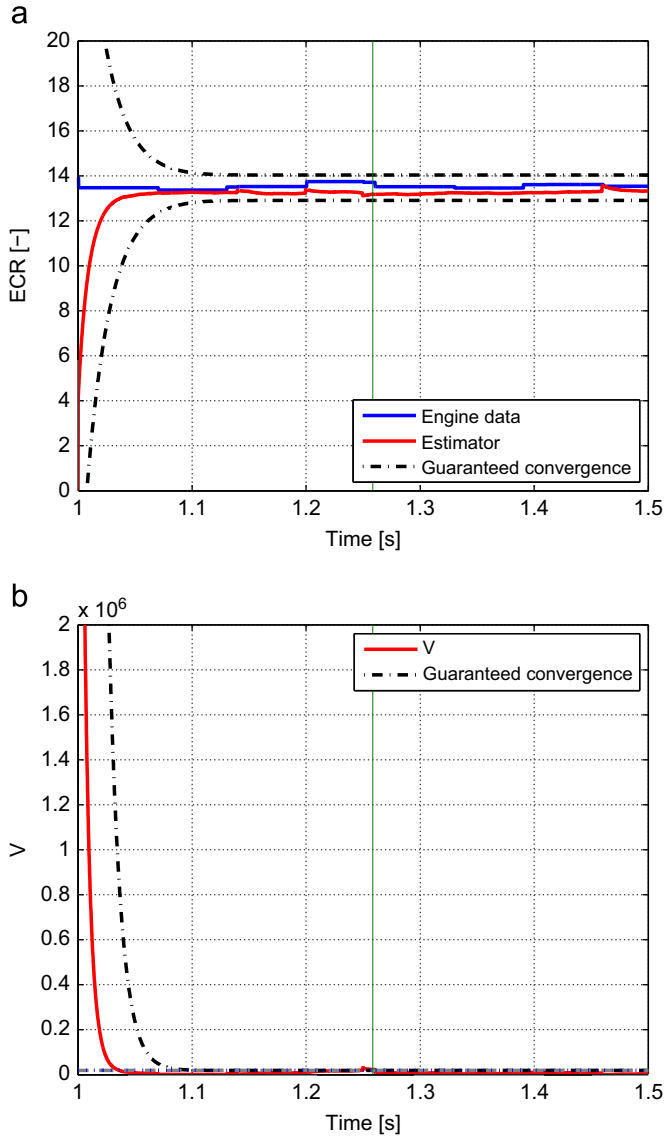

Fig. 24. Estimator convergence for Case 2: ECR ≈ 14. (a) ECR convergence and (b) squared error convergence. (For interpretation of the references to color in this figure legend, the reader is referred to the web version of this article.)

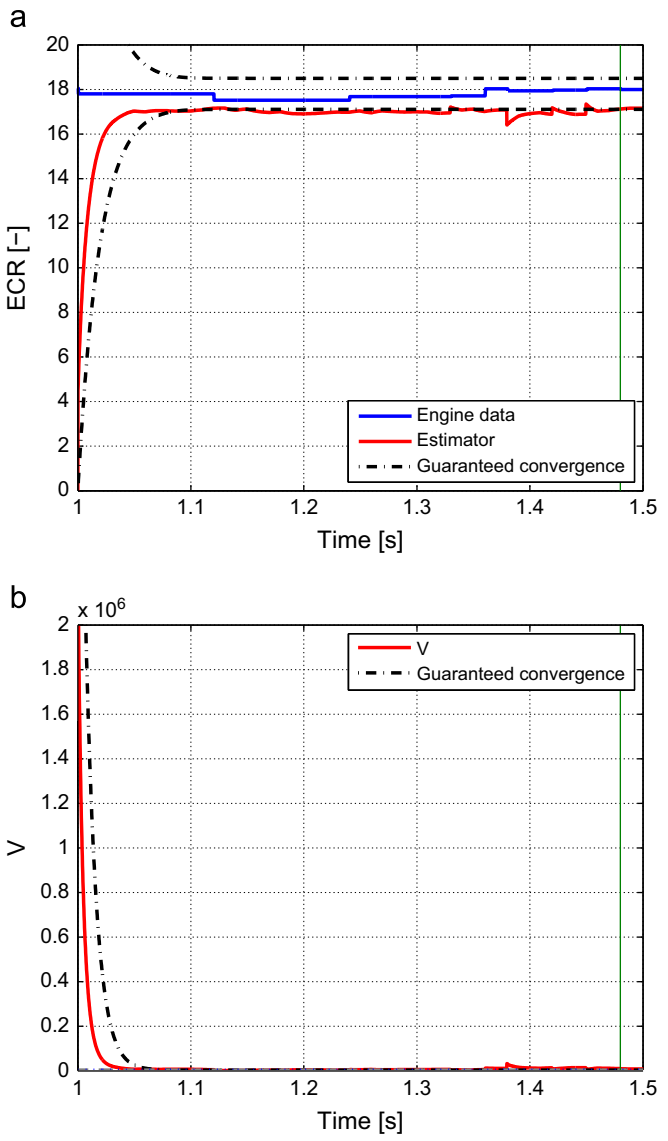

Fig. 25. Estimator convergence for Case 3: ECR ≈ 18. (a) ECR convergence and (b) squared error convergence. (For interpretation of the references to color in this figure legend, the reader is referred to the web version of this article.)

for the estimator to predict within 0.25 effective compression ratio of the true value, given the amount of measurement uncertainty in the system. If a larger error in effective compression ratio can be tolerated, then the gain may be decreased. Conversely, in order to handle larger amounts of uncertainty, higher gains are needed.

Note that these curves change not only for each operating condition, but also depend on the effective compression ratio. Based on this, the gain may change depending on operating condition, or one gain may chosen to satisfy requirements at all operating conditions.

As a conservative example, consider the system bounds corresponding to Case 5, Jump 2, with 10% uncertainty in EGR flow measurement, a typical error for the operating conditions considered in this study. For the application of estimating effective compression ratio, a reasonable error is assumed to be 0.5ECR. The authors in Modiyani et al. (2011) established a one-to-one relationship between volumetric efficiency and effective compression ratio, demonstrated in Fig. 20, and the corresponding change in volumetric efficiency is 0.03. Combining this along with the limits defined by engine operation and system dynamics (listed in Table 5), the observer gain is calculated using Eq. (47), as shown in Eq. (48), and a gain of 93 results

$$\kappa_e > \frac{404.5\ (\mathrm{kPa/s})}{0.03 \cdot 148\ \mathrm{kPa} - \frac{2 \cdot 0.287\ \mathrm{kJ/kg\ K} \cdot 60\ \mathrm{s}}{0.0067\ \mathrm{m^3} \cdot 2300\ \mathrm{rpm}} 0.1 \cdot 0.036\ (\mathrm{kg/min}) \cdot 366.9\ \mathrm{K}}$$

$$= 92.365\ \mathrm{s}^{-1} \tag{48}$$

Values of the observer gain calculated via Eq. (47) for the rest of the cases are also listed in Table 5, each gain calculated to handle up to 10% uncertainty in measurement of EGR flow. Also listed in Table 5 are values for κ_{t98}, assuming convergence was required within 4 engine cycles (see Table 2). Comparing the values for κ_{t98} with those for κ_e, the larger gain (rounded up) was chosen via Eq. (20) and listed in the κ column. As previously mentioned, the selected gain automatically satisfies the conditions imposed by the four factors of convergence time, system dynamics (i.e. $|\dot{x}|_{max}$), measurement uncertainty, and allowable steady-state error, per Eqs. (40) and (47).

For this study, the gains listed in Table 5 are calculated off-line and then implemented in subsequent tests. In practice, however,

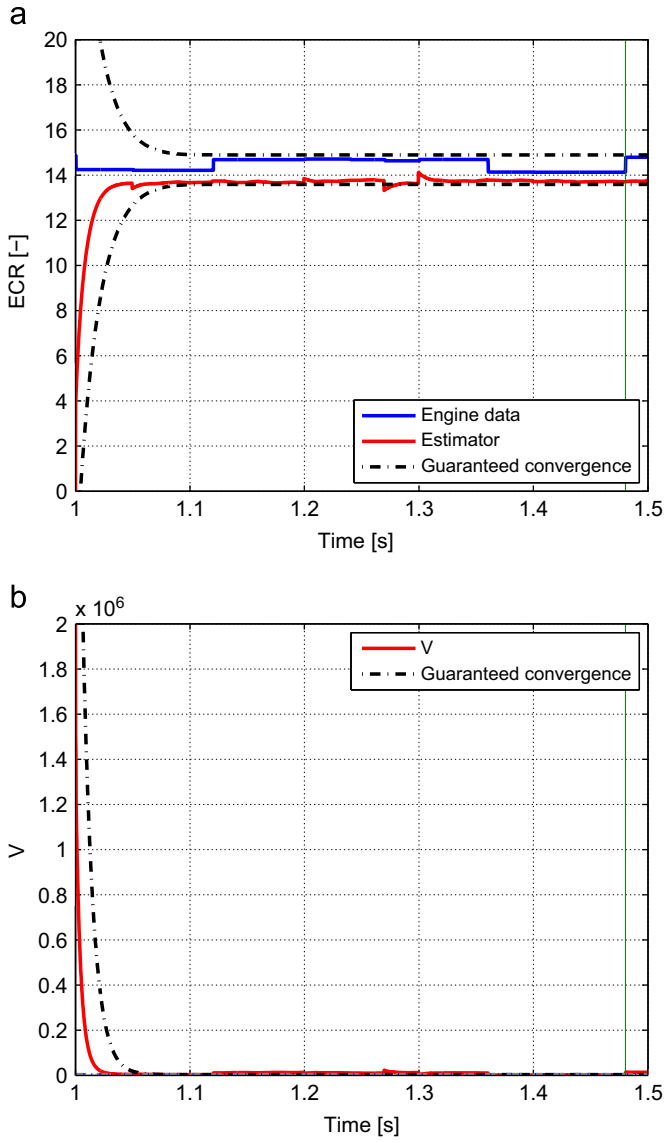

Fig. 26. Estimator convergence for Case 3: ECR ≈ 14. (a) ECR convergence and (b) squared error convergence. (For interpretation of the references to color in this figure legend, the reader is referred to the web version of this article.)

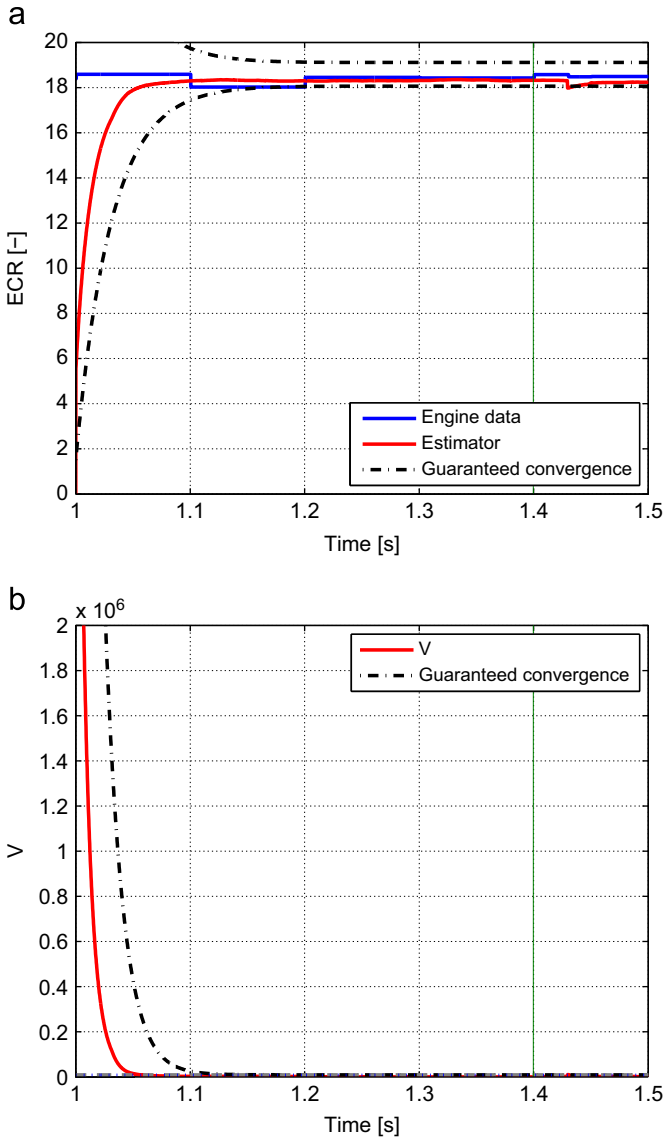

Fig. 27. Estimator convergence for Case 4: ECR ≈ 18. (a) ECR convergence and (b) squared error convergence. (For interpretation of the references to color in this figure legend, the reader is referred to the web version of this article.)

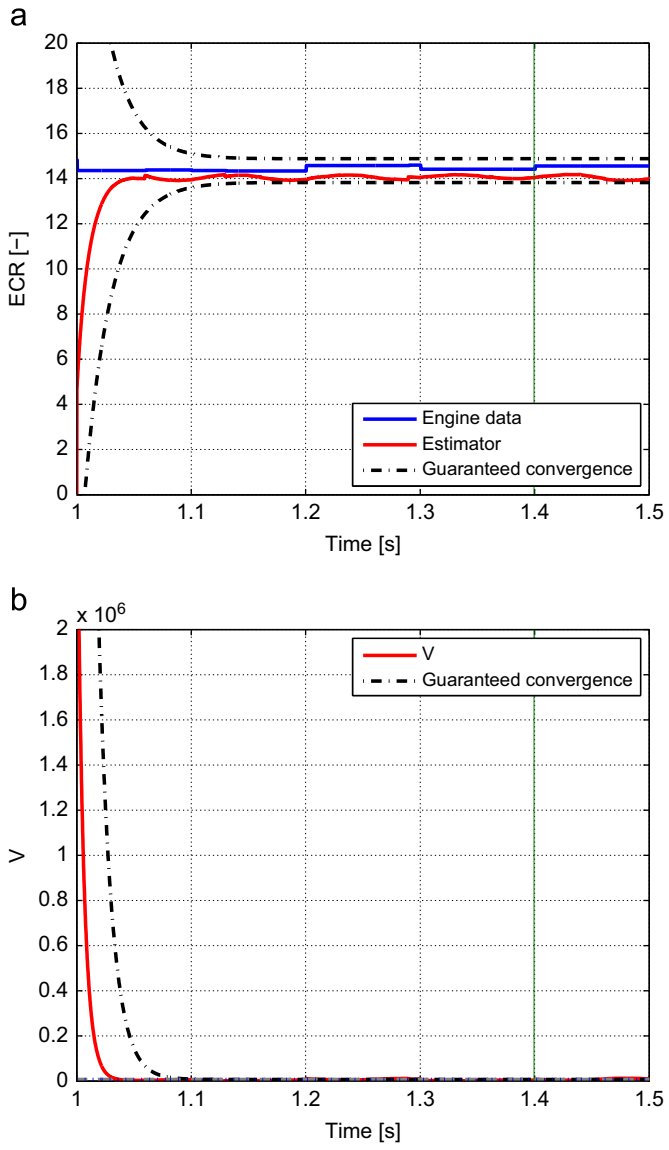

Fig. 28. Estimator convergence for Case 4: ECR ≈ 14. (a) ECR convergence and (b) squared error convergence. (For interpretation of the references to color in this figure legend, the reader is referred to the web version of this article.)

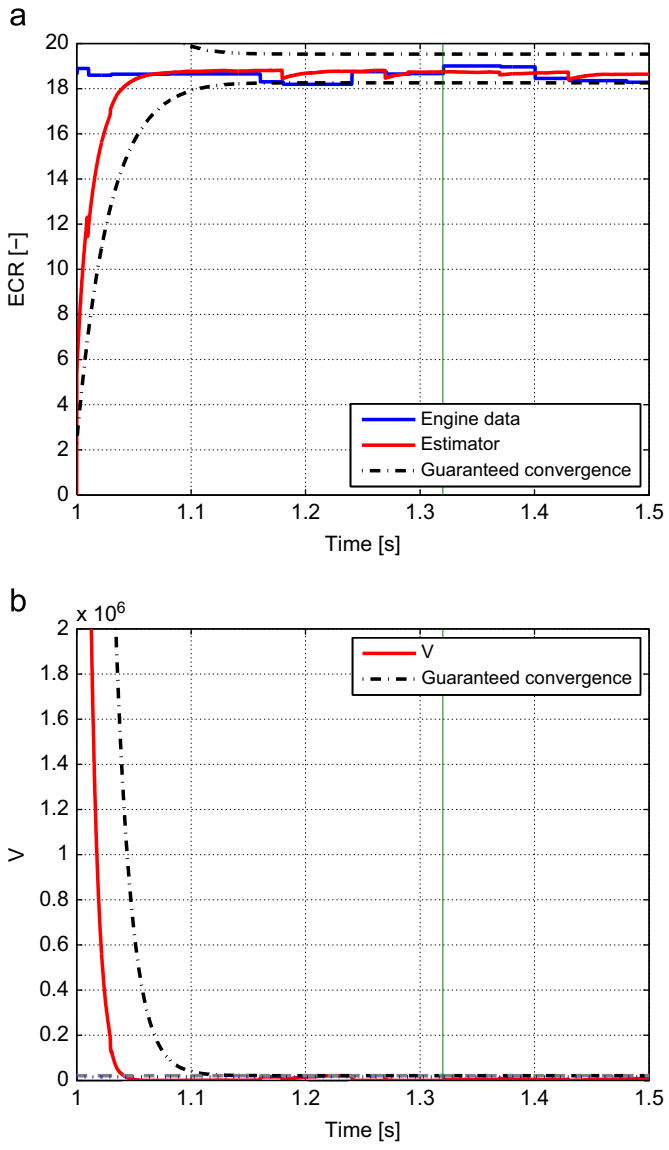

Fig. 29. Estimator convergence for Case 5: ECR ≈ 18. (a) ECR convergence and (b) squared error convergence. (For interpretation of the references to color in this figure legend, the reader is referred to the web version of this article.)

depending on the system and application, the gain may be calculated and adjusted within a control loop.

6. Experimental results: convergence and robustness

Figs. 21–30 demonstrate the convergence of the estimator, robust to EGR flow uncertainty. Each test uses the gains listed in Table 5. For these convergence tests, at each of the five operating points, the estimator was tested in steady-state for the two IVC timings listed in Table 4. The estimator was initially off, and after one second was turned on to test convergence in the worst case. The actual effective compression ratio, calculated using lab-grade in-cylinder pressure data, is plotted in blue in each subfigure (a), with estimator performance in red, and the dashed black line indicates the guaranteed convergence rate per Eq. (19), shown again in Eq. (49) with variables specific to this application included. The vertical green line in each of the figures indicates the time equivalent of four engine cycles at the speed of each operating point, and in all cases, the estimator converges well within four engine cycles.

$$V \le \left[V_0 - \frac{\left(\frac{\gamma_{im} V_d N}{2V_{im}}\right)^2 \left(\left|\frac{d(p_{im}\eta_v)}{dt}\right|_{max} + \frac{2\kappa R_{im} T_{egr}}{V_d N} |\Delta W_{egr}| \right)^2}{\kappa^2} \right] \exp(-\kappa t) + \frac{\left(\frac{\gamma_{im} V_d N}{2V_{im}}\right)^2 \left(\left|\frac{d(p_{im}\eta_v)}{dt}\right|_{max} + \frac{2\kappa R_{im} T_{egr}}{V_d N} |\Delta W_{egr}| \right)^2}{\kappa^2} \tag{49}$$

In subfigures (b), the convergence of the squared error is shown in red, compared to the guaranteed rate in dashed black. Again, the vertical green line indicates the 4-engine cycle time span for each operating condition. In all cases, the error converges to the acceptable steady-state error, shown in blue, well within the desired time frame, and in many cases converges to an even smaller error than that predicted by Eq. (49).

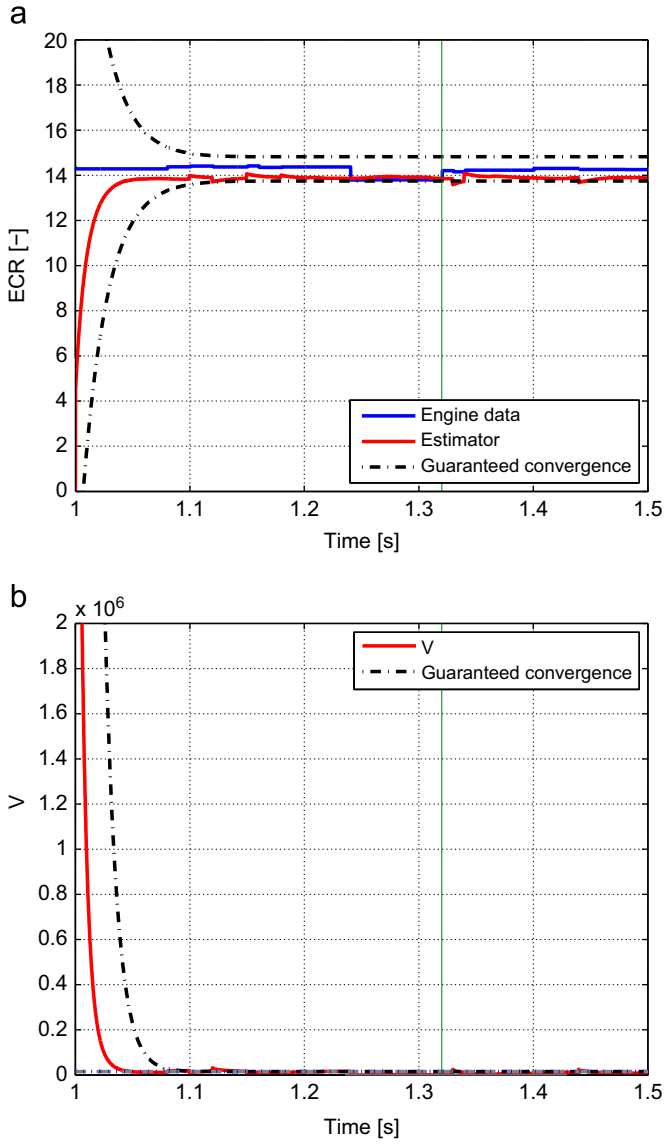

Fig. 30. Estimator convergence for Case 5: ECR ≈ 14. (a) ECR convergence and (b) squared error convergence. (For interpretation of the references to color in this figure legend, the reader is referred to the web version of this article.)

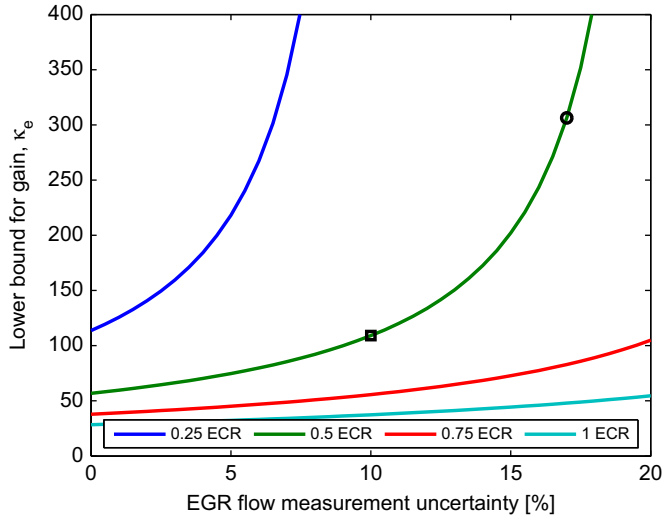

Fig. 31. Gain trade-off for Case 1: higher uncertainty.

7. The noise trade-off

In Sections 2 and 3, Lyapunov techniques were used to ensure exponential stability of the estimator and provided insight on selecting a reasonable lower bound for the observer gain to ensure the estimator was robust to uncertainty in EGR flow measurement while still converging to an acceptable ECR value in a desired amount of time. The relationship between these three, given by Eqs. (40) and (47) and shown again here

$$\kappa = \max \begin{pmatrix} \kappa_e > \dfrac{\sup_t \left| \dfrac{d}{dt}(p_{im}\eta_v) \right|}{|p_{im}(\eta_v - \hat{\eta}_v)| - \dfrac{2R_{im}}{V_d N} |\Delta(W_{egr} T_{egr})|} \\ \kappa_{t_{98}} \geq \dfrac{4N}{120n} \end{pmatrix} \tag{50}$$

indicates the trade-off that exists when determining how to select the observer gain. Again, this relationship was illustrated in Figs. 8 and 15–19. As previously mentioned, if a larger error in effective compression ratio can be tolerated, then the gain may be decreased. Conversely, in order to handle larger amounts of uncertainty, higher gains are needed. Additionally, by selecting the larger gain as directed

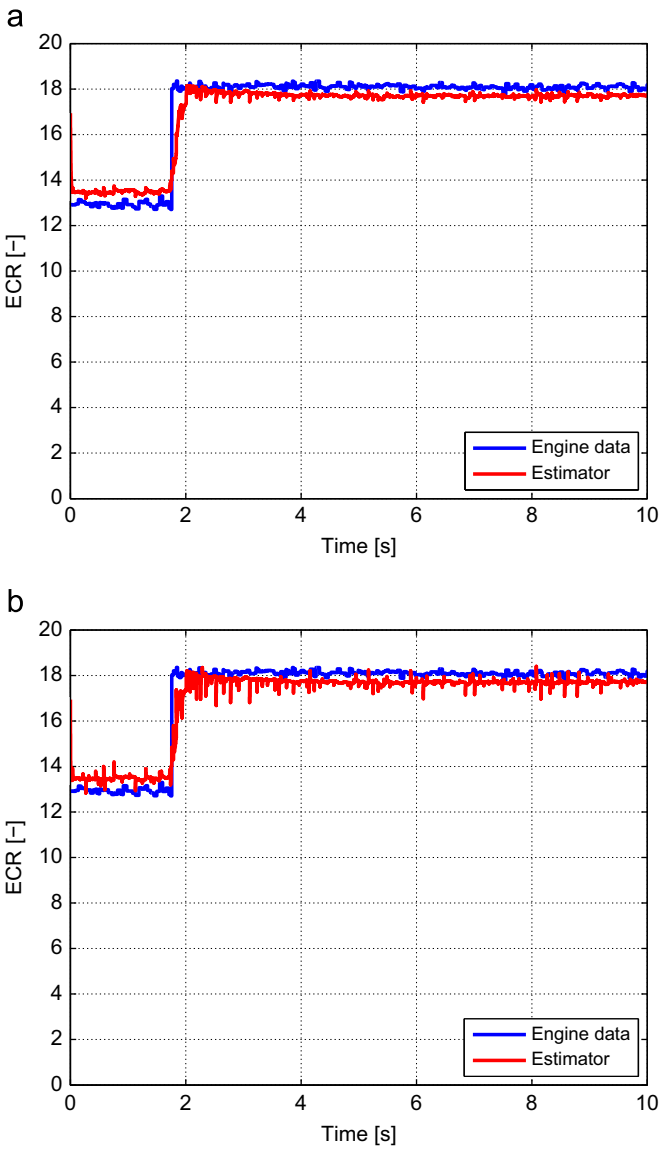

Fig. 32. Case 1 noise-gain trade-off: (a) original gain and (b) higher gain.

by Eq. (50), all the gain constraints (convergence time, measurement uncertainty, acceptable steady-state error) will be satisfied. The gain cannot, however, be increased without limit.

For example, consider the gain trade-off for Case 1, Jump 1. If the estimator was desired to handle up to 17% uncertainty in the measurement of EGR flow, a higher gain would be needed, as shown in Fig. 31. The required gain corresponding to 10% uncertainty for an acceptable ECR error of 0.5 is indicated by the black square, while the required gain corresponding to 17% uncertainty is marked with a black circle. The estimator was re-tested for the transient step change for this test (Case 1, Jump 1) with the corresponding increased gain for handling 17% uncertainty. Fig. 32(a) shows the estimator performance with the original gain, while Fig. 32(b) shows results with the increased gain, corresponding to moving from the square to the circle in Fig. 31. It is evident that the larger gain produces more noise in the estimated ECR signal than might be acceptable for control purposes. As such, there is a limit to how much the gain can be reasonably increased to accommodate measurement uncertainty. Currently there is no analytical tool to determine what this limit might be, and is an area for future investigation.

8. Conclusions and future work

A more aggressive (i.e. less conservative) lower bound for the error convergence rate of the high-gain input observer outlined in Stotsky and Kolmanovsky (2002) was developed, and takes into account the desired convergence time as well as measurement uncertainty and acceptable steady-state error. A trade-off between measurement uncertainty, acceptable error in effective compression ratio, and observer gain was also characterized to direct the selection of an appropriate gain value. These strategies were demonstrated in practice for the estimation of the effective compression ratio for IC engines incorporating flexible intake valve closing time modulation.

The ECR estimation scheme developed in Stricker et al. (2012) was analyzed for robustness to uncertainty in the EGR flow measurement, and was shown to handle up to 10% EGR flow uncertainty. In addition, the estimator was proven to exponentially converge to an acceptable region of error in effective compression ratio within a desired amount of time. The noise-gain trade-off study in Section 7 indicated limitations to gain increases for the purpose of handling uncertainty in EGR flow measurements. While an analytical method for determining a lower bound for the observer gain was presented, starting in Section 3, no analytical tool currently exists for determining an upper limit for the gain. An area for future work is investigating the development of such a tool, which will be greatly beneficial for implementation in control design.

Disclaimer

This report was prepared as an account of work sponsored by an agency of the United States Government. Neither the United States Government nor any agency thereof, nor any of their employees, makes any warranty, express or implied, or assumes any legal liability or responsibility for the accuracy, completeness, or usefulness of any information, apparatus, product, or process disclosed, or represents that its use would not infringe privately owned rights. Reference herein to any specific commercial product, process, or service by trade name, trademark, manufacturer, or otherwise does not necessarily constitute or imply its endorsement, recommendation, or favoring by the United States Government or any agency thereof. The views and opinions of authors expressed herein do not necessarily state or reflect those of the United States Government or any agency thereof.

Acknowledgments

This material is based upon work supported by the Department of Energy under Award Number DE-EE0003403.

Special thanks to Cummins, Inc. for providing the engine and other experimental equipment, as well as technical support, especially from the following researchers at Cummins Technical Center in Columbus, Indiana: Ray Shute, Tim Frazier, Cheryl Klepser, Don Stanton, Phanindra Garimella, and Rajani Modiyani. Special thanks, also, to AVL North America, Inc. for providing use of an AVL 621 Indimodul for the collection and analysis of in-cylinder pressure transducer data. The authors also wish to thank the Technical Services staff at the Ray W. Herric Laboratories for their assistance: Fritz Peacock, Bob Brown, Gil Gordon and Frank Lee.

Appendix A

In the following section, the transient bound for the estimation error given in Eq. (6) is shown. This proof was developed in correspondence with Prof. Ilya Kolmanovsky at the University of Michigan. As a reminder, consider a first-order system:

$$\dot{z} = y + x \tag{A.1}$$

where z and y are measured or known, x is to be estimated. The estimate of x is given by

$$\hat{x} = \kappa z - \varepsilon \tag{A.2}$$

where κ is the observer gain and ε satisfies

$$\dot{\varepsilon} = -\kappa\varepsilon + \kappa y + \kappa^2 z \tag{A.3}$$

To show $\hat{x}$ is a good approximation for x, consider the error between the two, given by e as

$$e = \hat{x} - x = \kappa z - \varepsilon - x \tag{A.4}$$

Taking the derivative of Eq. (A.4), together with Eqs. (A.1)–(A.3), yields

$$\dot{e} = \kappa\dot{z} - \dot{\varepsilon} - \dot{x} = -\kappa e - \dot{x} \tag{A.5}$$

For a physical system, the dynamics of the unknown variable x may be bounded, that is, for some constant $B_1 > 0$:

$$sup_t |\dot{x}(t)| \le B_1 \tag{A.6}$$

Multiplying Eq. (A.5) by $2e$ yields

$$2e\dot{e} = -2\kappa e^2 - 2e\dot{x} \tag{A.7}$$

Consider the last term in the above equation. The following inequality holds true:

$$-2\dot{x}e \le |2\dot{x}e| \tag{A.8}$$

Considering this along with the derivative of e^2, Eq. (A.7) becomes

$$\frac{d(e^2)}{dt} = 2e\dot{e} = -2\kappa e^2 - 2e\dot{x} \le -2\kappa e^2 + |2\dot{x}e|$$
$$\Rightarrow \frac{d(e^2)}{dt} \le -2\kappa e^2 + |2\dot{x}e| \tag{A.9}$$

Now a bound must be put on $|2\dot{x}e|$ in Eq. (A.9). Consider the following. For any two real numbers u and w, and any real number $c > 0$, the following inequality holds:

$$(|u| - c|w|)^2 \ge 0 \tag{A.10}$$

Expanding this inequality and rearranging terms yields:

$$0 \le (|u| - c|w|)^2 = |u|^2 - c|uw| - c|uw| + c^2|w|^2$$
$$\Rightarrow 0 \le u^2 - 2c|uw| + c^2w^2$$
$$\Rightarrow 2c|uw| \le u^2 + c^2w^2 \tag{A.11}$$

Solving for $|uw|$ results in the following inequality:

$$|uw| \le \frac{u^2}{2c} + \frac{c^2w^2}{2c} = \frac{u^2}{2c} + \frac{cw^2}{2}$$
$$\Rightarrow |uw| \le \frac{u^2}{2c} + \frac{cw^2}{2} \tag{A.12}$$

In the context of the high-gain observer problem, make the following assignments for:

$$u = \dot{x} \quad w = 2e \quad c = \frac{\kappa}{2} \tag{A.13}$$

Substituting these assignments into Eq. (A.12) yields

$$|\dot{x}(2e)| \le \frac{\dot{x}^2}{2\left(\frac{\kappa}{2}\right)} + \frac{\left(\frac{\kappa}{2}\right)(2e)^2}{2} = \frac{\dot{x}^2}{\kappa} + \frac{4\kappa e^2}{4}$$
$$\Rightarrow |2\dot{x}e| \le \frac{\dot{x}^2}{\kappa} + \kappa e^2 \tag{A.14}$$

Now Eq. (A.14) is substituted into Eq. (A.9) and the bound given in Eq. (A.6) is included to yield

$$\frac{d(e^2)}{dt} \le -2\kappa e^2 + |2\dot{x}e| \le -2\kappa e^2 + \frac{B_1^2}{\kappa} + \kappa e^2$$
$$\Rightarrow \frac{d(e^2)}{dt} \le -\kappa e^2 + \frac{B_1^2}{\kappa} \tag{A.15}$$

Separation of variables results in the following:

$$\frac{d(e^2)}{dt} \le -\kappa e^2 + \frac{B_1^2}{\kappa} = -\kappa\left(e^2 - \frac{B_1^2}{\kappa^2}\right)$$
$$\Rightarrow \frac{d(e^2)}{\left(e^2 - \frac{B_1^2}{\kappa^2}\right)} \le -\kappa\, dt \tag{A.16}$$

Both sides of this inequality are then integrated:

$$\int \frac{d(e^2)}{\left(e^2 - \frac{B_1^2}{\kappa^2}\right)} \le \int -\kappa\, dt \Rightarrow \ln\left|e^2 - \frac{B_1^2}{\kappa^2}\right| \le -\kappa t + \alpha_1 \tag{A.17}$$

To solve for e, the error between the estimate $\hat{x}$ and true value x, the exponential of both sides is taken and rearranged as follows:

$$e^2 - \frac{B_1^2}{\kappa^2} \le \exp(-\kappa t + \alpha_1) \Rightarrow e^2 - \frac{B_1^2}{\kappa^2} \le \alpha_2 \exp(-\kappa t)$$
$$\Rightarrow |e(t)| \le \sqrt{\alpha_2 \exp(-\kappa t) + \frac{B_1^2}{\kappa^2}} \tag{A.18}$$

Solving for α_2 by considering initial conditions:

$$|e(0)| \le \sqrt{\alpha_2 \exp(0) + \frac{B_1^2}{\kappa^2}} = \sqrt{\alpha_2 + \frac{B_1^2}{\kappa^2}} \tag{A.19}$$

Choosing $|e(0)| = \sqrt{\alpha_2}$, since $\sqrt{\alpha_2} < \sqrt{\alpha_2 + B_1^2/\kappa^2}$, results in

$$\alpha_2 = |e(0)|^2 = e(0)^2 = e_0^2 \tag{A.20}$$

Thus, Eq. (A.18) becomes

$$|e(t)| \le \sqrt{e_0^2 \exp(-\kappa t) + \frac{B_1^2}{\kappa^2}} \tag{A.21}$$

Then it is easy to see that in Eq. (A.4), for $t > 0$, the error in estimation of x becomes arbitrarily small for large κ, and $\hat{x}$ approaches x.

Consider also the case in which measurement uncertainty or noise is included on signals y or z in the system given by Eq. (A.1). For example, suppose

$$\dot{z} = y_{meas} + x \tag{A.22}$$

where y_{meas} is defined as

$$y_{meas} = y + \Delta y \tag{A.23}$$

with y being the true value and Δy being the noise or uncertainty in the measurement of the signal. The estimator design then becomes

$$\hat{x} = \kappa z - \varepsilon$$

$$\dot{\varepsilon} = -\kappa\varepsilon + \kappa y_{meas} + \kappa^2 z$$
$$= -\kappa\varepsilon + \kappa(y + \Delta y) + \kappa^2 z$$
$$= -\kappa\varepsilon + \kappa y + \kappa\Delta y + \kappa^2 z \tag{A.24}$$

Now consider the error between estimated and actual x:

$$e = \hat{x} - x = \kappa z - \varepsilon - x \tag{A.25}$$

Taking the derivative and including Eq. (A.24):

$$\dot{e} = \kappa\dot{z} - \dot{\varepsilon} - \dot{x}$$
$$= \kappa y + \kappa x + \kappa\varepsilon - \kappa y - \kappa\Delta y - \kappa^2 z - \dot{x}$$
$$= -\kappa^2 z + \kappa\varepsilon + \kappa x - \dot{x} - \kappa\Delta y$$
$$\Downarrow$$
$$\dot{e} = -\kappa e - \dot{x} - \kappa\Delta y = -\kappa e - (\dot{x} + \kappa\Delta y) \tag{A.26}$$

Similar to Eq. (A.7), Eq. (A.26) is multiplied by $2e$, and a bound similar to Eq. (A.8) is applied, resulting in:

$$2e\dot{e} = \frac{d(e^2)}{dt} = -2\kappa e^2 - 2e(\dot{x} + \kappa\Delta y)$$
$$\le -2\kappa e^2 + |2e(\dot{x} + \kappa\Delta y)| \tag{A.27}$$

where the last term can be bound following the same process given by Eqs. (A.10)– (A.14):

$$|2e(\dot{x} + \kappa\Delta y)| \le \frac{(\dot{x} + \kappa\Delta y)^2}{\kappa} + \kappa e^2 \tag{A.28}$$

With this bound, Eq. (A.27) then becomes

$$\frac{d(e^2)}{dt} \le -\kappa e^2 + \frac{(\dot{x} + \kappa\Delta y)^2}{\kappa} \tag{A.29}$$

Assigning an upper bound for system dynamics similar to Eq. (A.6):

$$sup_t|\dot{x} + \kappa\Delta y| \le B_{1\Delta} \tag{A.30}$$

with a worst-case value for $B_{1\Delta}$ given by

$$B_{1\Delta} = |\dot{x}|_{max} + \kappa||\Delta y| \tag{A.31}$$

the error dynamics in Eq. (A.29) become

$$\frac{d(e^2)}{dt} \le -\kappa e^2 + \frac{B_{1\Delta}^2}{\kappa} \tag{A.32}$$

Following the same steps laid out in Eqs. (A.16)–(A.21), a transient error bound is obtained:

$$\frac{d(e^2)}{dt} \le -\kappa\left(e^2 - \frac{B_{1\Delta}^2}{\kappa^2}\right)$$
$$\frac{d(e^2)}{\left(e^2 - \frac{B_{1\Delta}^2}{\kappa^2}\right)} \le -\kappa\, dt$$

$$\int \frac{d(e^2)}{\left(e^2-\frac{B_{1\Delta}^2}{\kappa^2}\right)} \le \int -\kappa\, dt \Rightarrow \ln\left|e^2-\frac{B_{1\Delta}^2}{\kappa^2}\right| \le -\kappa t+\alpha_1$$

$$e^2-\frac{B_{1\Delta}^2}{\kappa^2} \le \exp(-\kappa t+\alpha_1) \Rightarrow e^2-\frac{B_{1\Delta}^2}{\kappa^2} \le \alpha_2 \exp(-\kappa t)$$

$$\Rightarrow |e(t)| \le \sqrt{\alpha_2 \exp(-\kappa t)+\frac{B_{1\Delta}^2}{\kappa^2}}$$

$$|e(0)| \le \sqrt{\alpha_2 \exp(0)+\frac{B_{1\Delta}^2}{\kappa^2}} = \sqrt{\alpha_2+\frac{B_{1\Delta}^2}{\kappa^2}} \Rightarrow \text{let } \alpha = e_0^2$$

$$\Rightarrow |e(t)| \le \sqrt{e_0^2 \exp(-\kappa t)+\frac{B_{1\Delta}^2}{\kappa^2}} \tag{A.33}$$

and similar to Eq. (A.21), for large κ, the estimation error becomes small, but is now affected by the amount of measurement uncertainty, Δy.

References

Ahn, K., Stefanopoulou, A. G., & Jankovic, M. (2009). Tolerant ethanol estimation in flex-fuel vehicles during MAF sensor drifts. In *Proceedings of the*2009 *dynamic systems and control conference*.

Bartolini, G., Ferrara, A., & Stotsky, A. A. (1994). Exponential stability of a simplified adaptive control scheme in presence of bounded disturbances. In *Proceedings of the*33*rd conference on decision and control*.

Bartolini, G., Ferrara, A., & Stotsky, A. A. (1999). Robustness and performance of an indirect adaptive control scheme in presence of bounded disturbances. *IEEE Transactions on Automatic Control*, *44*(4), 789–793.

Bullinger, E., & Allgower, F. (1997). An adaptive high-gain observer for nonlinear systems. In *Proceedings of the*36*th conference on decision and control*.

Chitour, Y. (2002). Time-varying high-gain observers for numerical differentiation. *IEEE Transactions on Automatic Control*, *47*(9), 1569–1656.

Dabroom, A., & Khalil, H. K. (1997). Numerical differentiation using high-gain observers. In *Proceedings of the*36*th conference on decision and control* (pp. 4790–4795). San Diego, CA.

Gauthier, J. P., & Kupka, I. A. K. (1994). Observability and observers for nonlinear systems. *SIAM Journal on Control and Optimization*, *32*(4), 975–994.

He, X., & Durrett, R. P. (2008). *Late intake closing as an emissions control strategy at tier 2 bin 5 engine-out NO_x level*. SAE 2008-01-0637.

Helmantel, A., Gustavsson, J., & Denbratt, I. (2005). *Operation of DI diesel engine with variable effective compression ratio in HCCI and conventional diesel mode*. SAE 2005-01-0177.

Heywood, J. (1988). *Internal combustion engine fundamentals*. New York, NY, USA: McGraw-Hill.

Hountalas, D. T., Mavropoulos, G. C., & Kourbetis, G. (2005). Experimental investigation to develop a methodology for estimation the compression condition of DI diesel engines. *Energy Conversion and Management*, *47*(1), 1–18.

Jia, M., Xie, M., Wang, T., & Peng, Z. (2011). The effect of injection timing and intake valve close timing on performance and emissions of diesel PCCI engine with full engine cycle CFD simulation. *Applied Energy*, *88*(9), 2967–2975.

Khalil, H. K. (1999). *High-gain observers in nonlinear feedback control. Lecture Notes in Control and Information Sciences*, vol. 244. Berlin/Heidelberg: Springer pp. 249–268.

Khalil, H. K. (2008). High-gain observers in nonlinear feedback control. In *Proceedings of the international conference on control, automation and systems*.

Klein, M., & Eriksson, L. (2006). *Methods for cylinder pressure based compression ratio estimation*. SAE 2006-01-0185.

Kocher, L., Koeberlein, E., VanAlstine, D. G., Stricker, K., & Shaver, G. (2011). Physically-based volumetric efficiency model for diesel engines utilizing variable intake valve actuation. *International Journal of Engine Research*, *13*(2), 169–184.

Kolmanovsky, I., Sivergina, I., & Sun, J. (2006). Simultaneous input and parameter estimation with input observers and set-membership parameter bounding: *Theory and an automotive application*. *International Journal of Adaptive Control and Signal Processing*, *20*(5), 225–246.

Kulkarni, A. M., Stricker, K. C., Blum, A., & Shaver, G. M. (2008). *PCCI control authority of a modern diesel engine outfitted with flexible intake valve actuation*. SAE 2009-01-1882.

Lamaris, V. T., & Hountalas, D. T. (2009). Validation of a diagnostic method for estimating the compression condition of direct injection diesel engines. *IMechE Journal of Power and Energy*, *224*, 517–532.

Mahmoud, M. S., & Khalil, H. K. (2002). Robustness of high-gain observer-based nonlinear controllers to unmodeled actuators and sensors. *Automatica*, *38*(2), 361–369.

Modiyani, R., Kocher, L., Van Alstine, D. G., Koeberlein, E., Stricker, K., Meckl, P., et al. (2011). Effect of intake valve closure modulation on effective compression ratio and gas exchange in modern, multi-cylinder diesel engines. *International Journal of Engine Research*, *12*(6), 617–631.

Murata, Y., Kusaka, J., Kawano, D., Suzuki, Y. D., Ishii, H., & Goto, Y. (2008). *Miller-PCCI combustion in an HSDI diesel engine with VVT*. SAE 2008-01-0644.

Murata, Y., Kusaka, J., Odaka, M., Daisho, Y., Kawano, D., Suzuki, H., et al. (2007). Emissions suppression mechanism of premixed diesel combustion with variable valve timing. *International Journal of Engine Research*.

Nevin, R., Sun, Y., Manuel, A., Gonzalez, D., & Reitz, R. (2007). *PCCI investigation using variable intake valve closing in a heavy duty diesel engine*. SAE 2007-01-0903.

Polushin, I. G., Liu, P. X., & Lung, C.-H. (2008). Projection-based force reflection algorithm for stable bilateral teleoperation over networks. *IEEE Transactions on Instrumentation and Measurement*, *57*(9), 1854–1865.

Poznyak, A. S., Martinez-Guerra, R., & Osorio-Cordero, A. (2000). Robust high-gain observer for nonlinear closed-loop stochastic systems. *Mathematical Problems in Engineering*, *6*, 31–60.

Saberi, A., & Sannuti, P. (1990). Observer design for loop transfer recovery and for uncertain dynamical systems. *IEEE Transactions on Automatic Control*, *35*(8), 878–897.

Stotsky, A., & Kolmanovsky, I. (2001). Simple unknown input estimation techniques for automotive applications. In *Proceedings of the American control conference*.

Stotsky, A., & Kolmanovsky, I. (2002). Application of input estimation techniques to charge estimation and control in automotive engines. *Control Engineering Practice*, *10*(12), 1371–1383.

Stotsky, A., Kolmanovsky, I., & Eriksson, S. (2004). Composite adaptive and input observer-based approaches to the cylinder flow estimation in spark ignition automotive engines. *International Journal of Adaptive Control and Signal Processing*, *18*(2), 125–144.

Stricker, K., Kocher, L., Koeberlein, E., VanAlstine, D. G., & Shaver, G. M. (2012). Estimation of effective compression ratio for engines utilizing flexible intake valve actuation. *Proceedings of the IMechE Part D: Journal of Automobile Engineering*, *226*(8), 1001–1015.

Tona, P., Moulin, P., Venturi, S., Tilagone, R., & Gautier, P. (2007). Towards integrated powertrain control for a mild-hybrid urban vehicle with a downsized turbo-charged CNG engine. *Oil and Gas Science and Technology*, *62*(4), 595–613.

Veluvolu, K. C., & Soh, Y. C. (2009). High-gain observers with sliding mode for state and unknown input estimations. *IEEE Transactions on Industrial Electronics*, *56*(9), 3386–3393.

Watzenig, D., Steiner, G., & Sommer, M. S. (2008). Robust estimation of blow-by and compression ratio for large diesel engines based on cylinder pressure traces. In *Proceedings of the 2008 IEEE international instrumentation and measurement technology conference*.